Materials Today Bio 32 (2025) 101831

Contents lists available at ScienceDirect

Materials Today Bio

journal homepage: www.journals.elsevier.com/materials-today-bio

Xanthohumol bulk-modified polyurethane for tracheal repair: A 'killing two birds with one stone' strategy for tailorable mechanics and durable anti-inflammatory efficacy

Siqiang Zheng [a,1], Li Xu [a,1], Qitao Bo [a], Erji Gao [a], Enkuo Zheng [b], Lei Xie [c], Bin Zhao [d], Jiaoyu Yi [e], Yang Li [g], Yong Xu [a,*], Yao Wang [a,f,**], Bo Tao [a,***]

[a] Department of Thoracic Surgery, Shanghai Pulmonary Hospital, Tongji University School of Medicine, Shanghai, 200443, China
[b] The Second Hospital of Ningbo, Ningbo, 315010, China
[c] Department of Thoracic Surgery, The Second Affiliated Hospital of Nanchang University, Nanchang, 330006, China
[d] Department of Pulmonary Nodule Center, Shandong Public Health Clinical Center, Jinan, 250100, China
[e] Department of Plastic Surgery, Renji Hospital, Shanghai Jiaotong University, School of Medicine, Shanghai, 200127, China
[f] Department of Cardiovascular Surgery, Zhongshan Hospital, Fudan University, Shanghai, 200032, China
[g] Shibei Hospital, Jing'an District, Shanghai, 201209, China

ARTICLE INFO

Keywords:
Bulk modification
Mechanical compliance
Long-lasting effect
Xanthohumol
Tracheal repair

ABSTRACT

Restoring tracheal defects remains a significant challenge in tissue engineering and regenerative medicine. Current scaffolds fall short of achieving optimal tracheal repair due to unmatched mechanical properties and limited anti-inflammatory properties. In this study, we incorporated the natural plant-derived anti-inflammatory molecule Xanthohumol (XN) into the backbone of a degradable polyurethane (PEUU) to create a porous PEXUU scaffold with tailorable mechanical properties and sustained anti-inflammatory activity. Materials Studio software was initially employed to simulate the feasibility of synthesizing the PEXUU elastomer using XN as a chain extender and poly(ε-caprolactone) as the soft segment. Mechanical tests confirmed the synthesized PEXUU elastomer exhibited excellent elasticity and fatigue resistance that closely mimic the mechanical properties of the natural trachea. The PEXUU elastomers were then processed into porous scaffolds via thermally induced phase separation, exhibited high porosity and favorable hydrophilicity while providing durable XN release kinetic in a sustained manner during degradation. *In vitro* co-culture studies demonstrated that the scaffold not only exhibited favorable biocompatibility and supported cartilage regeneration but also effectively downregulated pro-inflammatory factor expression and promoted the polarization of M1 macrophages toward the M2 phenotype. Furthermore, *in vivo* experiments revealed that implantation of the PEXUU scaffold significantly alleviated local inflammation and facilitated the formation of mature cartilage tissue. In a rabbit tracheal window defect model, the scaffold markedly reduced granulation tissue formation and preserved luminal patency, ultimately yielding excellent repair outcomes. In conclusion, XN bulk-modified PEUU represents a dual-function strategy that combines tailorable mechanical compliance with sustained anti-inflammatory activity. This approach significantly promotes tracheal regeneration and repair, offering promising prospects for clinical application.

1. Introduction

Congenital deformities, trauma and diseases often result in tracheal defects. Due to the trachea's continuous respiratory function and the specific mechanical stresses it endures under physiological conditions, conventional treatments—such as autologous grafts and prosthetic

This article is part of a special issue entitled: Multiscale Composites published in Materials Today Bio.

* Corresponding author.
** Corresponding author. Department of Thoracic Surgery, Shanghai Pulmonary Hospital, Tongji University School of Medicine, Shanghai, 200443, China.
*** Corresponding author.
E-mail addresses: xuyong@tongji.edu.cn (Y. Xu), wang.yao1@zs-hospital.sh.cn (Y. Wang), tbo0820@163.com (B. Tao).
[1] Those authors are equal to this work.

https://doi.org/10.1016/j.mtbio.2025.101831
Received 24 March 2025; Received in revised form 27 April 2025; Accepted 3 May 2025
Available online 8 May 2025

implants—frequently fail to yield satisfactory clinical outcomes [1]. Consequently, repairing tracheal defects remains challenging because of the complexity inherent in tracheal structure and function. Tissue engineering, by effectively integrating biomaterials with seed cells, holds significant promise for developing tracheal substitutes that closely mimic the native trachea's structure and function, thus offering a novel solution for tracheal reconstruction [2,3].

Selecting suitable biomaterials requires an in-depth understanding of normal tracheal biomechanics and the microenvironment. Native tracheal cartilage exhibits a stiffness ranging between 1 and 39 MPa, enabling it to withstand cyclic compression and tension during respiration [4]. Therefore, an ideal engineered tracheal scaffold must strike a delicate balance—rigid enough to support ventilation yet flexible enough to accommodate airway bending and stretching [5]. Additionally, since tracheal transplants are continuously exposed to the external environment, they are highly susceptible to infection, potentially compromising the healing process [6]. Consequently, an optimal tissue-engineered tracheal scaffold must possess both suitable mechanical properties and anti-inflammatory functions to prevent infection and support repair, thus overcoming current limitations.

Recent developments in biomaterial-based tissue engineering have renewed interest in porous scaffolds for tracheal repair [7,8]. Despite advancements, clinical translation remains elusive. Current tracheal scaffolds are predominantly fabricated from either natural or synthetic polymers. Natural polymers—such as collagen, hyaluronic acid, and decellularized extracellular matrix (ECM)—offer superior biocompatibility and effectively replicate the native cartilage ECM environment, but their insufficient mechanical strength limits clinical application [6,9]. Conversely, synthetic polymers like polylactic acid (PLA) and polyglycolic acid demonstrate high mechanical strength; however, their excessive rigidity exemplified by PLA's Young's modulus exceeding 3 GPa, results in mechanical mismatch with native tracheal cartilage [10,11]. Thus, synthetic polymers typically fail to adequately accommodate the respiratory system's cyclical compression and tension. To overcome these challenges, the ideal tracheal scaffold should exhibit optimal mechanical adaptability, balancing radial stiffness with longitudinal flexibility.

Furthermore, the in-situ regeneration and restoration of tracheal cartilage faces substantial inflammatory challenges, primarily driven by four factors: 1) Scaffold materials and their degradation by-products trigger foreign body reactions [12]; 2) Dedifferentiation of chondrocytes during *in vitro* expansion leads to immunogenic changes [13,14]; 3) Surgical trauma activates inflammatory cascades [15]; and 4) External exposure of the tracheal environment increases infection risk, exacerbating inflammation [16]. Previous anti-inflammatory strategies, such as prolonged *in vitro* culture or epithelial lining development [17,18], have limitations, including increased operational complexity or donor-site morbidity. Additionally, strategies involving bioactive materials like strontium-doped bioactive glass or curcumin-based hydrogels have not consistently achieved stable cartilage regeneration in immunocompetent animal models [19,20]. Zhou et al. reported significant ECM erosion in approximately 40 % of engineered cartilage implants due to macrophage infiltration in large animal models [21]. Traditional strategies typically rely on short-term drug release, resulting in rapid *in vivo* clearance and inadequate sustained inflammation suppression. Hence, developing a scaffold with sustained anti-inflammatory effects and mechanical adaptability is crucial to overcome existing limitations.

Biodegradable polyurethane (BDPU) represents a promising biomaterial for tracheal tissue engineering due to its tunable molecular structure, allowing precise modulation of mechanical properties. By carefully adjusting the hard-to-soft segment ratio through suitable chain extenders, BDPU can mimic native tracheal tissue's anisotropic mechanical behavior, ensuring radial rigidity and longitudinal flexibility [22]. Nevertheless, current functionalization strategies face a paradox: physical blending methods cause rapid drug release, whereas chemical grafting methods exhibit stable drug retention but limited loading capacity [23,24]. Recently, incorporating bioactive molecules directly into the BDPU backbone has been explored, exemplified by integrating salvianolic acid A as a chain extender, resulting in sustained immunomodulatory effects during myocardial repair [25]. Inspired by this innovative approach, we propose a "dual-function" strategy: selecting bioactive drug molecules with both anti-inflammatory properties and reactive functional groups as chain extenders, covalently embedding them into the polyurethane backbone. This molecular engineering approach ensures simultaneous mechanical adaptability and sustained anti-inflammatory efficacy through coupled drug release and scaffold degradation.

Xanthohumol (XN), a natural flavonoid derived from hops, exhibits robust anti-inflammatory and antioxidant activities [26]. Its structural components—particularly isoprenoid and α, β-unsaturated carbonyl groups—contribute significantly to its antibacterial and anti-inflammatory effects [27]. The presence of hydroxyl groups in XN theoretically enables covalent integration into polyurethane structures as chain extenders [28]. Thus, incorporating XN into the BDPU backbone to produce a novel XN-modified BDPU (PEXUU) scaffold may concurrently deliver mechanical adaptability and sustained anti-inflammatory activity, thereby effectively suppressing local inflammation.

In this study, we synthesized an innovative PEXUU elastomer by incorporating XN into the polyurethane backbone via in situ bulk polymerization. We subsequently fabricated porous scaffolds through thermally induced phase separation (TIPS) and systematically evaluated their performance in terms of: (1) optimized mechanical adaptability, achieving elasticity and fatigue resistance through synergistic interactions between XN and polyurethane segments; (2) sustained anti-inflammatory efficacy via synchronized XN release and scaffold degradation; and (3) comprehensive assessment of biocompatibility, cartilage regeneration potential, and efficacy of defect repair using a rabbit tracheal window-defect model (Scheme 1). This research aims to present a novel tracheal scaffold with improved mechanical adaptability and long-term anti-inflammatory capabilities, offering significant potential for clinical application in tracheal repair.

2. Materials and methods

2.1. Molecular dynamics simulation analysis of PEXUU molecules

In this study, molecular dynamics simulations were performed using the COMPASS II force field to model all components. Internal hydrogen bonds were classified and statistically analyzed. The dynamic functionality of the Forcite module was then employed to simulate the random motion of PEXUU molecules within the lattice, with force field parameters describing hydrogen bond interactions. Analysis of the trajectory files yielded Mean Squared Displacement (MSD) and Radial Distribution Function (RDF) curves.

To maintain thermodynamic equilibrium, both Andersen temperature and pressure regulators were used, and the velocity Verlet algorithm was applied with a time step of 1 fs. Each system was equilibrated for 500 ps over a temperature range of 300 K–500 K, ensuring that the molecular chains fully relaxed and reached their lowest-energy state. The final equilibrium structures were subsequently used for further structural and property analyses.

2.2. Preparation of PEXUU elastomers via bulk modification of XN into the BDPU backbone

Initially, 5 g of polycaprolactone diol (PCL diol; Sigma, USA) was placed in a three-necked flask and slowly heated to 120 °C under vacuum to remove water. The flask was then cooled to 80 °C. Under a nitrogen atmosphere, 1,6-hexamethylene diisocyanate (HDI; Shanghai Titan Scientific Co., Ltd.) was gradually added to initiate

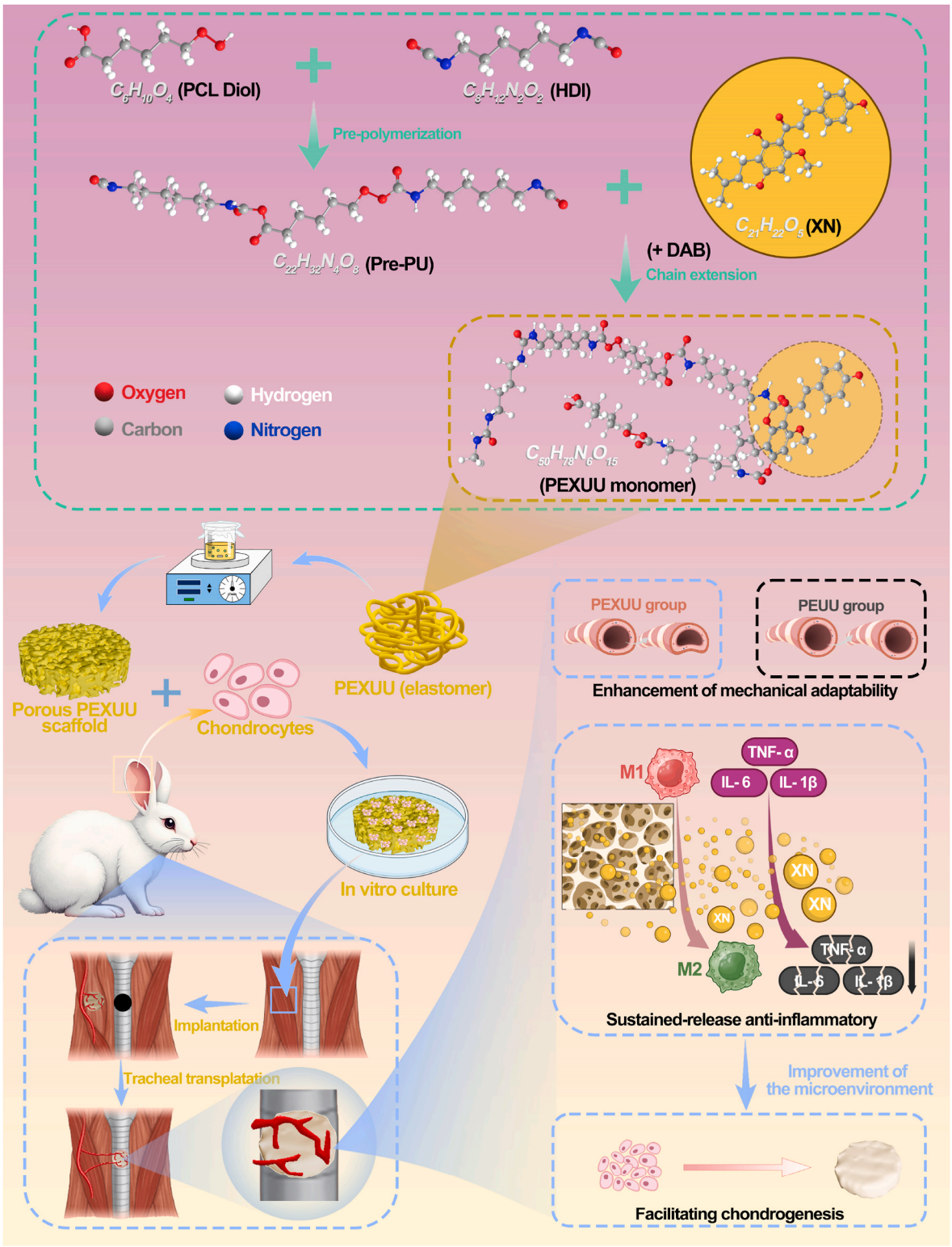

Scheme 1. Schematic illustration of the design of PEXUU porous scaffolds via bulk modification of XN into polyurethane backbone, giving rise to tailorable mechanics and durable anti-inflammatory efficacy for tracheal repair. In step 1, PCL-diol and HDI undergo a prepolymerization reaction to form Pre-PU. In step 2, XN acts as a chain extender, reacting with Pre-PU to yield the bulk-modified PEXUU elastomer. This elastomer is then processed into a porous scaffold using the TIPS method. The resulting PEXUU scaffold demonstrates excellent mechanical adaptability, closely mimicking that of the natural trachea. Furthermore, the sustained release of XN from the scaffold optimizes the immune microenvironment by inducing a phenotypic shift in macrophages—from the M1 pro-inflammatory phenotype to the M2 anti-inflammatory phenotype—which reduces inflammation and promotes chondrogenesis. Together, the scaffold's mechanical adaptability and durable anti-inflammatory effects synergistically facilitate the repair of tracheal defects.

prepolymerization.

After prepolymerization, a DMSO (TCI, Japan) solution containing XN (Shanghai Yuanye Biotechnology Co., Ltd.) and 1,4-diaminobutane (DAB; Sigma, USA) was slowly introduced according to the ratio specified in Table S1. The reaction mixture was maintained at 80 °C for 2 h and then cooled to 40 °C for 24 h to facilitate chain extension. Finally, the product was brought to room temperature, precipitated, washed with ice-cold deionized water, and freeze-dried to constant weight. Based on the varying XN content, the products were designated as PEUU, PEXUU-25, PEXUU-50, PEXUU-75, and PEXUU-100.

2.3. Characterization and evaluation of PEXUU elastomers

The purified PEXUU elastomers were weighed, and synthesis yield percentages were calculated using the formula: $(M_p/(M_{PCL} + M_{HDI} + M_{XN} + M_{DAB}) \times 100\ \%)$, where M_p is the weight of the purified product, and M_{PCL}, M_{HDI}, M_{XN}, and M_{DAB} represent the masses of PCL-OH, HDI, XN, and DAB used, respectively.

Morphological characteristics and preliminary mechanical properties were assessed by photographing the elastomer samples against a uniform background and performing simple break tests on samples of consistent size. Standard tensile tests were conducted in accordance with ISO 527-1 and ASTM D412 standards using a high-precision tensile testing machine (HY-025CS; Shanghai Hengyu Instrument Co., Ltd.). Dumbbell-shaped samples (ISO 37 Type 3) with a 20 mm gauge length were tested at a loading rate of 50 mm/min under constant room temperature. Tensile force and displacement were recorded to generate complete stress-strain curves.

Fourier-transform infrared (FTIR) spectroscopy was employed to verify the successful incorporation of the active drug XN onto the PEUU backbone. Samples of PCL, HDI, Pre-PU, XN, and PEXUU were placed in contact with an ATR crystal, and spectra were recorded over the range of 500–4000 cm^{-1} at a resolution of 4 cm^{-1} with 32 scans using a Nicolet IS20 FTIR spectrometer.

Additionally, ^{1}H Nuclear Magnetic Resonance (^{1}H NMR) spectroscopy was used to analyze the molecular structures of Pre-PU, XN, and PEXUU. Samples dissolved in deuterated DMSO were scanned using a Bruker 400M NMR spectrometer.

Thermal stability was assessed via thermogravimetric analysis (TGA). Approximately 5 mg of each sample was heated from 30 °C to 600 °C at a rate of 10 °C/min under a nitrogen atmosphere (20 mL/min). Thermogravimetric and differential thermogravimetric (DTG) curves were recorded for analysis.

2.4. Preparation of porous PEXUU scaffolds

PEUU and PEXUU elastomer solutions were prepared by dissolving the polymers in DMSO at mass concentrations of 4 %, 6 %, 8 %, and 10 % (w/v). The solutions were heated in a water bath at 80 °C until they became clear, and the dissolution process was monitored and recorded.

For a control solution (PEUU/X), 0.94 g of PEUU was dissolved in 10 mL of DMSO. The solution was heated to 80 °C with continuous stirring until clear, after which 60 mg of XN powder was added, resulting in a solution with a relative mass fraction of 6 %.

Porous scaffolds were then fabricated from the PEUU/X, PEUU, and PEXUU solutions using the TIPS method. First, a polytetrafluoroethylene mold (10 mm diameter, 2 mm height) was ultrasonically cleaned and refrigerated. The clear solution was maintained at 80 °C and gently stirred to induce foaming before being quickly poured into the pre-cooled mold. The mold was immediately transferred to a −20 °C freezer and left overnight.

The following day, the mold was removed from the freezer and immersed in a 0 °C ice-water bath to remove the separated solvent; the water was replaced every 4 h. Once the solvent was sufficiently removed, the scaffold was carefully extracted using tweezers and immersed in deionized water for 48 h to eliminate residual solvent. Finally, the scaffold was pre-frozen at −80 °C for 4 h and then freeze-dried to yield the porous scaffolds.

2.5. Characterization of porous PEXUU scaffolds

2.5.1. Morphological analysis

Porous scaffolds of PEUU and PEXUU, prepared at various concentrations, were photographed from different angles using a single-lens reflex camera (Fuji, Japan). Selected samples were cryo-fractured with liquid nitrogen, and their cross-sections were gold-coated for 60 s. Scanning electron microscopy (SEM) was then performed at an acceleration voltage of 10 kV to examine the scaffold morphology. The resulting SEM images were analyzed with ImageJ software to determine the pore size distribution across different concentrations.

2.5.2. Porosity measurement

The porosity of the scaffolds was determined using the liquid displacement method. First, 5 mL of anhydrous ethanol was accurately measured and recorded as V_1. Next, a freeze-dried scaffold was immersed in the ethanol for 10 min, and the total volume after immersion was recorded as V_2. The scaffold was then removed, and the remaining ethanol volume in the sealed graduated cylinder was measured as V_3 to prevent evaporation. Porosity was calculated using the formula: $(V_2 - V_3)/V_1 \times 100\ \%$.

2.5.3. Hydrophilicity assessment

The hydrophilicity of the scaffolds was assessed by measuring the water contact angle with a contact angle goniometer. A 0.03 mL droplet of deionized water was carefully placed on the scaffold surface, and the contact angle was recorded 5 s after deposition.

Cylindrical samples (10 mm diameter and 5 mm height) of the scaffolds were prepared to evaluate water absorption. The dry weight (W_0) was recorded before immersing the samples in deionized water at room temperature for 2 h. After immersion, the samples were gently blotted with filter paper to remove excess water and then reweighed (W_1). The water absorption rate was calculated as follows: $(W_1 - W_0)/W_0 \times 100\ \%$.

The total amount of protein adsorbed on PEUU and PEXUU scaffolds was determined using a modified bicinchoninic acid protein test as described previously [29]. The amount of adsorbed protein on the scaffolds was measured with a BCA protein assay kit (Beyotime, China).

2.5.4. Mechanical testing

Mechanical properties were evaluated using a high-precision tensile testing machine (HY-025CS, Shanghai Hengyu Instrument Co., Ltd.). Cylindrical scaffolds (10 mm diameter and 5 mm height) were first immersed in phosphate-buffered saline (PBS) for 2 h. The samples were then compressed at a rate of 2 mm/min until a strain of 50 % was reached, and stress–strain curves were recorded.

Another set of samples underwent cyclic compression tests. These samples were compressed at 2 mm/min to 40 % strain and then allowed to recover at 5 mm/min to 0 % strain for 20 cycles. Stress–strain curves were recorded for each cycle, and the peak stress was extracted. All tests were performed with the samples kept wet, and each group was tested in triplicate. Young's modulus was calculated from the stress–strain curves using Origin software. The stress residual rate was determined using the formula: $(\sigma_{20}/\sigma_1) \times 100\ \%$, where σ_1 is the peak stress in the first cycle and σ_{20} is the peak stress in the 20th cycle.

2.5.5. XN quantification

To prepare a stock solution, 10 mg of XN powder was dissolved in 10 mL of 50 % ethanol to yield a concentration of 1 mg/mL. Serial dilutions were then performed using a 50 mL volumetric flask to obtain standard solutions with concentrations of 8, 16, 24, 32, 40, 48, 56, and 64 μg/mL. The XN content in these solutions was measured using an Agilent 1260 Infinity high-performance liquid chromatography (HPLC) system at 370

nm. The analysis parameters were as follows: an injection volume of 10 μL, a column temperature of 40 °C, a flow rate of 1 mL/min, and a mobile phase comprising a 50:50 ethanol/water mixture. A standard curve was generated by plotting peak area against XN concentration for subsequent quantitative analysis of XN release.

2.5.6. Degradation studies

For degradation studies, PEUU, PEUU/X (6 % w/v), and PEXUU (6 % w/v) scaffolds were cut into 100 mg samples and freeze-dried to remove residual solvents. Samples were immersed in 5 mL of PBS (pH 7.4) and incubated at 37 °C in a constant-temperature shaker (100 rpm). At time points of 0, 2, 4, 8, 12, 16, 20, and 24 weeks, samples were retrieved, washed with deionized water, and freeze-dried. The remaining mass was calculated using: $(M_t/M_0) \times 100$ %, where M_0 is the initial mass and M_t is the mass at a given time point. Using 80 μg/mL proteinase K (Shanghai Biyuntian Biotechnology Co., Ltd.), 100 mg samples from each group were placed in 5 mL of PBS (pH 7.4) containing the enzyme and incubated at 37 °C with shaking at 100 rpm. Samples were collected at the same time points as above, washed, freeze-dried, and weighed. The remaining mass was calculated similarly to the hydrolytic degradation experiment.

At each time point, the enzymatic degradation solution was filtered through a 0.45 μm membrane to remove particulates, and the XN concentration was measured using the previously described HPLC conditions. The cumulative XN release was calculated using: $(\Sigma(C_i \times V)/M_{XN}) \times 100$ %, where C_i is the concentration of XN in the i-th collected degradation solution (μg/mL), V is the volume of the degradation solution (mL), and M_{XN} is the initial amount of XN in the sample (μg). Pearson correlation analysis was then performed to assess the relationship between mass loss percentage and cumulative XN release over time.

2.6. Biocompatibility evaluation of porous PEXUU scaffolds

Healthy 2-month-old New Zealand white rabbits (both male and female, weighing 2.0 ± 0.2 kg; provided by Shanghai Yunde Biotechnology Co., Ltd.) were used in this study. All experimental protocols (No. K21-355Y) were approved by the Ethics Committee of Shanghai Pulmonary Hospital. For isolation, each rabbit was anesthetized and placed in the lateral position, and approximately 60 % of the ear tissue was excised; the incision was then sutured. The excised tissue was disinfected in 75 % alcohol for 5 min, washed three times with PBS, and transferred to a sterile laminar flow hood. Under sterile conditions, the skin and connective tissue were removed, and the tissue was cut into 1 mm^3 pieces. These pieces were washed, digested with trypsin for 20 min, and rinsed with Dulbecco's Modified Eagle Medium (Sigma, USA). Next, collagenase was added for overnight digestion. The resulting cell suspension was filtered and centrifuged to isolate the chondrocytes, which were then seeded at a density of 1×10^6 cells per plate in 10-cm culture dishes. The cells were cultured at 37 °C in a 5 % CO_2 atmosphere, with the medium changed every 3 days. When the cells reached 80–90 % confluence, they were passaged by washing, trypsin digestion, neutralization, centrifugation, resuspension, and re-plating at the same density. Passage 2 (P2) cells were used for scaffold seeding.

Biocompatibility experiments were conducted with three groups: 1) Pure chondrocytes (control); 2) PEUU + chondrocytes; 3) PEXUU + chondrocytes. The PEUU and PEXUU porous scaffolds were sterilized with ethylene oxide. P2 chondrocytes were seeded onto the scaffolds at a density of 2×10^6 cells/mL, and the scaffolds were placed in 24-well plates and cultured at 37 °C with 5 % CO_2. For the control group, cells were directly seeded into 24-well plates. The culture medium was replaced every 2 days.

Live/dead cell staining was performed at predetermined time points. Cells were incubated with calcein AM and propidium iodide for 20 min, washed, and then examined using a laser confocal microscope. Cell viability was quantified using ImageJ software.

For cytoskeletal staining, cells were fixed, permeabilized, and blocked before staining. Rhodamine-phalloidin (Solarbio, Beijing, China) was used to stain the cytoskeleton, while 4′,6-diamidino-2-phenylindole (DAPI, Sigma, USA) stained the nuclei. The stained samples were imaged and photographed using a laser confocal microscope.

Cell proliferation was assessed using the Cell Counting Kit-8 (CCK-8, Sigma, USA) on days 1, 3, 5, and 7. After discarding the culture medium, scaffolds were washed twice with PBS, and 500 μL of a 10 % CCK-8 working solution was added. Samples were incubated in the dark for 2 h, after which 100 μL of the solution was transferred to a 96-well plate, and the optical density (OD) was measured at 450 nm.

DNA content was determined by grinding the scaffold in liquid nitrogen, followed by overnight digestion with proteinase K solution at 56 °C. After centrifugation, the supernatant was transferred to a 96-well plate. DNA content was quantified by measuring fluorescence intensity at 520 nm using a DNA assay kit (Thermo Fisher, USA) and a standard curve.

2.7. In Vitro anti-inflammatory performance of porous PEXUU scaffolds

RAW264.7 macrophages (obtained from the Chinese Academy of Sciences Shanghai Cell Bank, China) were pretreated with lipopolysaccharide (LPS, Sigma, USA) for 24 h to induce inflammation. Subsequently, the LPS-treated macrophages were cocultured with sterilized XN, and porous PEUU and PEXUU scaffolds were placed in 24-well plates at a density of 1×10^5 cells per well. For controls, macrophages without LPS treatment were seeded in 24-well plates under identical conditions.

After 48 h of coculture, the expression of inflammatory cytokines—including interleukin-6 (IL-6), interleukin-1β (IL-1β), and tumor necrosis factor-α (TNF-α)—was evaluated by immunofluorescence staining. Macrophages were collected, washed three times with PBS, and permeabilized with 0.1 % Triton X-100 for 20 min before being washed again. Following a 30-min blocking step with 5 % bovine serum albumin (BSA, Sigma, USA), primary antibodies against IL-6, IL-1β, and TNF-α were added and incubated overnight at 4 °C. After washing, macrophages were incubated with fluorescent secondary antibodies for 1–2 h, and DAPI was used to stain the nuclei. Images were captured using an inverted fluorescence microscope, and the relative intensities of IL-6, IL-1β, and TNF-α were quantified with ImageJ software.

Gene expression of pro-inflammatory cytokines (IL-6, IL-1β, and TNF-α), as well as CD206 and INOS, was analyzed by reverse transcription polymerase chain reaction (RT-PCR). During RNA extraction, scaffolds were frozen in liquid nitrogen, homogenized in lysis buffer, and centrifuged. RNA was purified using a gDNA filter column and the HiPure RNA Mini Column, then stored at −80 °C. cDNA was synthesized, and quantitative RT-PCR was performed as detailed in Tables S2 and S3. The PCR amplification cycle comprised an initial denaturation at 95 °C for 60 s, followed by 40 cycles of 95 °C for 15 s, 60 °C for 60 s, and 72 °C for 45 s (see Table S4). Relative mRNA expression was calculated using the $2^{\Delta\Delta CT}$ method. Primers were designed with Oligo software and verified using BLAST (Table S5).

2.8. In Vitro and In vivo cartilage formation

P2 chondrocytes were seeded at a density of 1×10^8 cells per scaffold onto sterile porous PEUU and PEXUU scaffolds to form chondrocyte–scaffold composites. The composites were cultured in a 37 °C incubator with the culture medium changed every three days. Samples were harvested for further analysis after 2 and 4 weeks of *in vitro* culture.

For the *in vivo* study, the ear-excised rabbits in section 2.6 were anesthetized, and the composites were implanted subcutaneously on both sides of the rabbits' backs. After 2 and 6 weeks of implantation, the composites were retrieved for morphological and biochemical analyses.

For morphological evaluation, the composites were washed with PBS, gently blotted to remove excess moisture, and digitally photographed. Cartilage thickness and height were measured using a caliper,

and the samples were weighed on an electronic balance.

Histological evaluation included Hematoxylin and Eosin (HE) staining, Safranin-O staining, and immunohistochemistry for type II collagen (COL II). For HE staining, cartilage tissue was fixed in 4 % paraformaldehyde for 4 h, automatically embedded, dehydrated through graded ethanol, and paraffin-embedded. Sections (5 μm) were baked at 60 °C overnight, then deparaffinized, rehydrated, stained with hematoxylin, differentiated, blued, counterstained with eosin, and mounted. Images were captured under a microscope. For Safranin-O staining, sections were immersed in a 0.2 % Safranin-O solution, dehydrated through graded ethanol, and mounted for observation. Immunohistochemistry for COL II involved deparaffinization, treatment with 3 % hydrogen peroxide, antigen retrieval in citrate buffer at 92–98 °C for 10–15 min, blocking with BSA, incubation with primary antibodies, treatment with secondary antibodies, DAB staining, and mounting. Images were then captured under a microscope. Additionally, heart, liver, spleen, lung, and kidney samples from the PEUU and PEXUU groups were subjected to HE staining for biosafety assessment, using samples from normal rabbits as controls.

Biochemical analysis involved quantifying glycosaminoglycan (GAG) content using the dimethylmethylene blue (DMMB) assay after digesting tissue samples with proteinase K (Beyotime, Shanghai, China). GAG content was determined using a standard curve from a DMMB assay kit (Biocolor, UK). COL II content was measured using an enzyme-linked immunosorbent assay kit (Sanying, Wuhan, China) by reading absorbance at 492 nm and quantifying according to a standard curve.

2.9. In vivo anti-inflammatory performance of porous PEXUU scaffolds

Subcutaneous tissue samples were collected from the rabbits' backs at 2 and 6 weeks post-implantation, as described in Section 2.8. Immunofluorescence staining was used to assess macrophage phenotypes—CD68, CD206, and INOS—and inflammatory cytokines IL-6, IL-1β, and TNF-α.

Briefly, paraffin sections were deparaffinized and rehydrated through graded alcohols, then incubated with 3 % hydrogen peroxide at room temperature for 10–15 min to block endogenous peroxidase activity. Next, the sections were immersed in citrate buffer and heated at 92–98 °C for 10–15 min for antigen retrieval. After three washes with PBS, sections were permeabilized with 0.1 % Triton X-100 for 20 min, rinsed with PBS, and blocked with 5 % BSA for 30 min. The sections were then incubated overnight at 4 °C with primary antibodies against CD68, CD206, INOS, IL-6, IL-1β, and TNF-α. Following another wash, fluorescent secondary antibodies were applied for 1–2 h, and the nuclei were counterstained with DAPI. Finally, the stained sections were examined using an inverted fluorescence microscope, and fluorescence intensities were quantitatively analyzed using ImageJ software.

2.10. Window-defect tracheal repair using Chondrocyte–Scaffold composites

Window-defect tracheal repair experiments were conducted using the ear-excised rabbits in section 2.6. Cartilage–scaffold composites prepared from PEUU and PEXUU (as described in Section 2.8) were first implanted into the subcutaneous spaces of the neck muscles for 4 weeks to induce pre-vascularization.

During surgery, the rabbits were anesthetized and placed in the supine position. A midline cervical incision was made to expose the trachea, and the pre-vascularized cartilage graft was carefully mobilized while preserving the muscle flap for blood supply. A 10-mm circular (window-shaped) defect was created between the 6th and 8th tracheal cartilage rings. The graft was trimmed and sutured into place using 6-0 absorbable sutures. After suturing, the surgical site was inspected for bleeding or air leakage, and the incision was closed in layers. The survival of the experimental rabbits was monitored for 8 weeks postoperatively.

At 4 weeks post-surgery, tracheal patency was evaluated via high-definition tracheal endoscopy in both the PEUU and PEXUU groups. The repaired tracheal tissue was bisected for morphological observation. Mechanical testing was performed by cutting the repaired and normal tracheal tissues into 2-mm-diameter pieces, measuring their height, and compressing the samples at a rate of 10 mm/min until 50 % strain was reached. Stress–strain curves were recorded, and the Young's modulus was calculated. Histological analyses were performed using HE and Safranin-O staining to evaluate primary cartilage features, as well as immunofluorescence staining for COL II and cytokeratin to assess cartilage-specific ECM formation and epithelialization. For biochemical analysis, COL II protein levels in the repaired tissues from both PEUU and PEXUU groups, as well as in normal tracheal tissue, were quantified using the method described in Section 2.8.

2.11. Statistical analysis

Statistical analyses were performed using SPSS version 19.0 software. Data from at least three independent experiments are presented as mean ± standard deviation (SD). Multiple comparisons were conducted using the Tukey post-hoc test, while two-way ANOVA was employed for comparisons among multiple groups. Comparisons between two groups were made using Student's t-test. Statistical significance was set at $*p < 0.05$.

3. Results

3.1. Molecular dynamics simulation analysis of PEXUU elastomer

As illustrated in Fig. S1, we designed a prepolymer of PEUU using PCL diol and HDI. During the chain extension reaction, the anti-inflammatory drug XN was incorporated into the PEUU main chain, thereby synthesizing the PEXUU elastomer.

Materials Studio software was employed to perform dynamic fitting analysis of the PEXUU polymer segments and to evaluate the newly generated carbamate groups. Fig. S2a shows that the PEXUU molecular chains synthesized from PCL diol, HDI, and XN exhibit good chemical stability and spatial flexibility. To analyze hydrogen bonding within the structure, we calculated the RDF for hydrogen and oxygen atoms capable of forming hydrogen bonds using molecular dynamics simulation. By analyzing both the MSD and RDF, we obtained microscopic insights into polymer chain motion and atomic interactions, thereby elucidating the relationship between internal microstructure and mechanical properties. As shown in Fig. S2b, at 800 ps the molecular chain mobility of PEXUU50 and PEXUU75 increases significantly—indicating enhanced segment flexibility and superior compressive properties—whereas PEUU exhibits the lowest MSD, reflecting reduced mobility. Fig. S2c reveals that although the RDF peaks for PEUU and PEXUU occur at similar distances (primarily reflecting hydrogen bonds between carbamate linkages), the higher peak in PEUU indicates stronger hydrogen bonding due to a greater carbamate linkage density. Moreover, Fig. S2d–e demonstrate that the RDF values for both N-H and O-H hydrogen bonds are higher in PEUU than in PEXUU; however, in PEXUU the RDF increases with the XN ratio, suggesting a looser internal structure and improved elasticity. Compression simulations show that PEUU has a significantly higher Young's modulus than PEXUU (Fig. S2f), while PEXUU exhibits excellent rebound performance—making it particularly suitable for tissues with retractile properties, such as the trachea.

3.2. Characterization evaluation of PEXUU elastomers

Fig. 1a displays the macroscopic morphology of PEXUU elastomers synthesized at four different molar ratios. The results indicate that although PEXUU can be synthesized using XN as a chain extender over a range of feed ratios, continuous globular formations only appear when

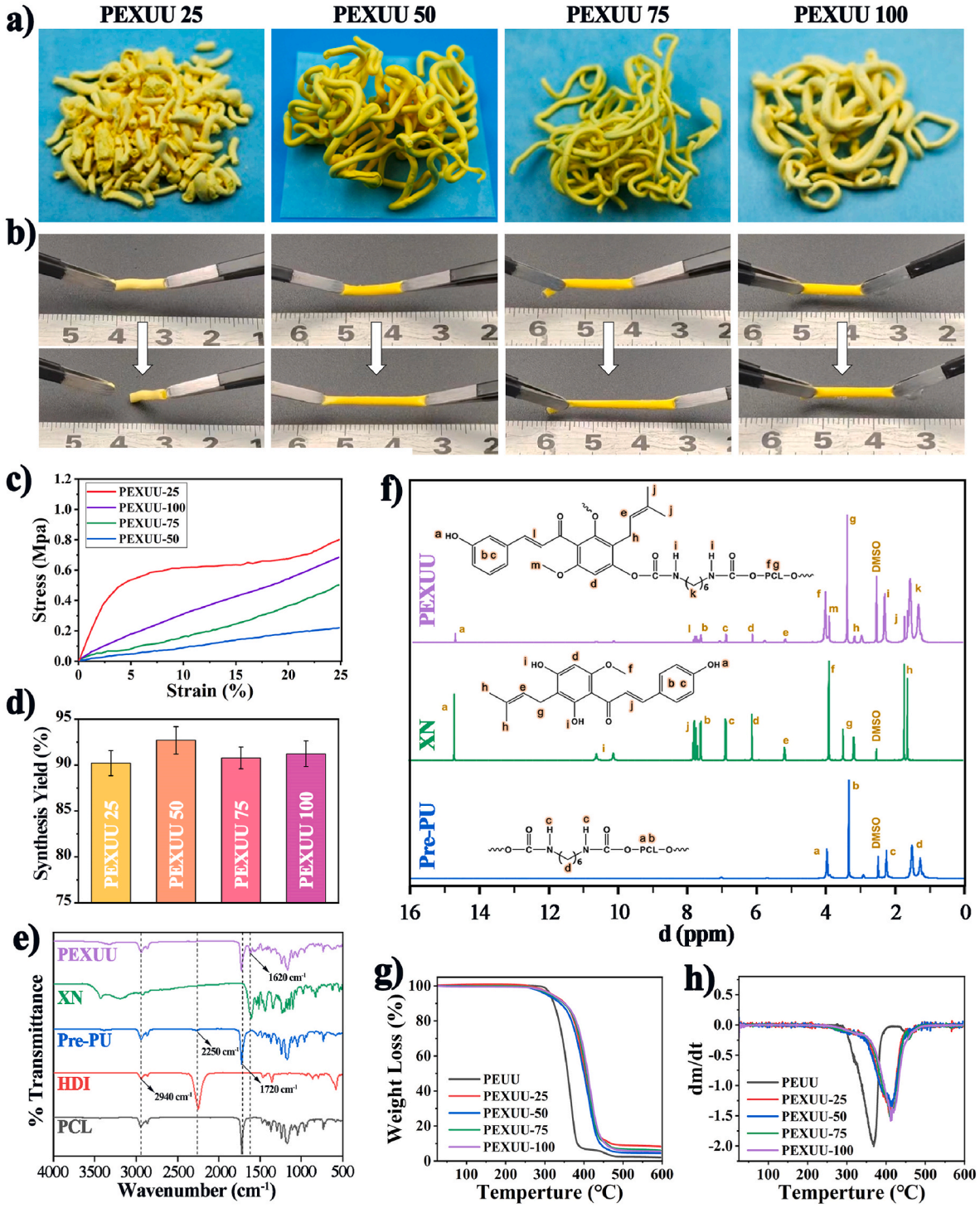

Fig. 1. Synthesis and characterizations of PEXUU elastomers with different XN contents. (a) Macroscopic morphology of PEXUU elastomers with different XN contents. (b) Photographs illustrating the tensile properties of PEXUU elastomers with different XN contents. (c) Stress-strain curves of PEXUU elastomers with different XN contents. (d) Synthesis yield percentages of PEXUU elastomers with different XN contents. (e) FTIR spectra of HDI, PCL-diol, Pre-PU, XN, and PEXUU. (f) 1H NMR spectra of Pre-PU, XN, and PEXUU. (g) TGA of PEUU and PEXUU in various XN contents groups. (h) DTG analysis of PEUU and PEXUU in various XN contents group.

the XN content exceeds 50 %. Notably, the elastomer produced at 50 % group exhibits the most complete morphology and uniform texture, corresponding to the highest molecular weight and reaction efficiency. Mechanical testing (Fig. 1b and c) further shows that increasing the XN content gradually improves tensile performance, reaching an optimum at a 50 % feed ratio—a finding consistent with the molecular dynamics simulation. Because XN is not entirely linear in structure, using it exclusively as a chain extender leads to incomplete reactions and reduced molecular weight, thereby diminishing elasticity.

Synthesis yield evaluation (Fig. 1d) indicates that all four PEXUU formulations achieve yields above 90 %, with the PEXUU50 formulation reaching the highest yield (92.7 ± 1.49 %). This confirms the feasibility of using XN as a small-molecule chain extender and underscores the importance of optimizing composition ratios. Consequently, PEXUU-

50—exhibiting the best rebound performance and yield—was selected as the scaffold material for subsequent studies.

FTIR analysis (Fig. 1e) shows that the prepolymer (Pre-PU) displays a characteristic peak at 2940 cm^{-1} (attributed to the carbon chains of PCL and HDI) and a carbonyl absorption peak at 1720 cm^{-1} (corresponding to the urethane linkage), confirming the successful synthesis of Pre-PU and enabling XN incorporation. After adding XN, PEXUU exhibits a distinct absorption peak at 1620 cm^{-1} due to the benzene ring, which verifies that XN successfully acted as a chain extender and was embedded in the polyurethane main chain.

^{1}H NMR analysis (Fig. 1f) of Pre-PU reveals absorption peaks at 1.55, 3.34, and 3.97 ppm, corresponding to the carbon chains of PCL and HDI, along with a peak at 2.24 ppm indicating the reaction between isocyanate and hydroxyl groups. The presence of multiple characteristic peaks of XN in the PEXUU spectrum confirms its successful incorporation into the main chain.

TGA curve shows that the thermal decomposition temperature increases from 312.14 °C for unextended PEUU to 376.48 °C for XN-extended PEXUU (Fig. 1g). This improvement is attributed to the benzene ring in XN, which enhances chain stability, molecular entanglement, and hydrogen bonding. The DTG curve (Fig. 1h) indicates that the maximum pyrolysis peak of PEXUU (with various XN ratios) is higher than that of PEUU (362 °C) with minimal differences among the PEXUU samples, demonstrating that even a small amount of XN significantly improves thermal stability. Overall, PEXUU meets the thermal stability requirements for biomedical materials.

3.3. Performance analysis of porous PEXUU scaffolds

Our results indicate that at 80 °C, PEXUU solutions at 4 %, 6 %, 8 %, and 10 % concentrations dissolve completely to form pale yellow, transparent liquids (Fig. 2a). The macroscopic morphology of porous PEXUU scaffolds fabricated via TIPS is similar across concentrations, exhibiting a richly porous yellow surface (Fig. 2b). SEM reveals a homogeneous, interconnected pore structure (Fig. 2c). Pore size analysis (Fig. 2d) shows that, at a given concentration, PEXUU scaffolds have significantly larger internal pores than PEUU scaffolds, whose pore size decreases with increasing concentration. The largest average pore size for PEXUU scaffolds (89.15 ± 7.48 μm) was observed at 6 % concentration. Porosity measurements (Fig. 2e) indicate that increasing the preparation concentration reduces porosity in both scaffold types, yielding a more compact structure. Notably, the porosity of the 4 % and 6 % PEXUU scaffolds is similar (92.21 ± 2.98 % vs. 90.84 ± 2.45 %, with no significant difference). These results suggest that the TIPS technique using a single solvent is effective for producing PEXUU scaffolds with porous structures conducive to cell proliferation and nutrient exchange.

Hydrophilicity was assessed via water contact angle, water absorption, and protein adsorption tests. PEXUU scaffolds exhibit contact angles ranging from 60° to 80° at 5 s, with the 6 % group having the smallest angle (64 ± 1.63°), indicative of superior hydrophilicity (Fig. 2f and g). In contrast, PEUU scaffolds show contact angles between 80° and 120° at 5 s—with lower concentrations yielding higher angles—demonstrating inferior hydrophilicity (Fig. 2g; see also Fig. S3). Water absorption tests reveal that PEUU scaffolds absorb 247–372 % of water after 24 h in PBS (with absorption inversely related to concentration), whereas PEXUU scaffolds exhibit much higher absorption: 1377.7 ± 46.5 % at 4 %, 910.3 ± 36.2 % at 6 %, 504.5 ± 28.8 % at 8 %, and 495.5 ± 20.86 % at 10 %. Additionally, our results indicate that the PEXUU group exhibited significantly higher protein adsorption capacity than the PEUU group at both 6 and 18 min (Fig. S4). Thus, XN modification markedly enhances the hydrophilicity of PEXUU.

Compression stress–strain testing demonstrates that the maximum stress at 50 % compression increases with scaffold concentration for both PEUU and PEXUU (Fig. 2i); however, the Young's modulus of PEUU scaffolds is significantly higher than that of PEXUU scaffolds (Fig. 2j). The linear stress–strain curve observed for PEXUU scaffolds indicates superior elasticity and rebound performance, making them well suited for tracheal cartilage tissue engineering. Moreover, cyclic compression tests (Fig. S5a–d) reveal that at 40 % compression, PEXUU scaffolds suffer significantly less stress loss than PEUU scaffolds. After 10 cycles, the stress retention in the PEUU group is 87.86 ± 2.68 %, whereas PEXUU scaffolds at 4 %, 6 %, 8 %, and 10 % concentrations retain 98.44 ± 2.11 %, 88.10 ± 1.27 %, 87.35 ± 3.56 %, and 85.28 ± 0.99 % of their initial stress, respectively (Fig. S5e). These findings confirm the excellent rebound and fatigue resistance of PEXUU scaffolds.

Degradation studies were performed by monitoring mass loss over 24 weeks. Under hydrolytic conditions in PBS (Fig. 2k), PEUU scaffolds lose 41.7 ± 4.3 % of their mass, reflecting the slowest degradation—consistent with stronger hydrogen bonding observed in RDF analysis. In contrast, PEUU/X scaffolds lose 60.8 ± 4.5 %, and PEXUU scaffolds show the highest degradation rate with a mass loss of 78.2 ± 6.0 %, demonstrating that XN modification effectively accelerates degradation and offers controlled biodegradability. Under enzymatic degradation in a proteinase K solution (Fig. 2l), PEUU scaffolds degrade by 45.9 ± 4.9 %, PEUU/X by 67.2 ± 5.3 %, and PEXUU scaffolds are completely degraded within 24 weeks.

Fig. 2m presents the cumulative and theoretical release profiles of XN from PEUU/X and PEXUU scaffolds over 24 weeks. PEUU/X scaffolds rapidly release 60.3 ± 3.7 % of XN within the first week and 79.6 ± 4.8 % by week 2, after which the release rate declines markedly. In contrast, PEXUU scaffolds exhibit a gradual, sustained release, with 42.7 ± 3.5 % cumulative release by week 4, 80.5 ± 4.6 % by week 12, and nearly 100 % by week 24—slightly exceeding the theoretical release curve. Finally, Pearson correlation analysis (Fig. 2n) between mass loss during enzymatic degradation and cumulative XN release from PEXUU scaffolds yields a linear regression ($Y = 1.039X + 5.967$) with a correlation coefficient of $r = 0.9852$, indicating a strong positive linear relationship.

3.4. In Vitro biocompatibility evaluation of porous PEXUU scaffolds

Chondrocytes were seeded onto both PEUU and PEXUU scaffolds, and live/dead staining was performed on days 1, 3, 5, and 7 (Fig. 3a). Both scaffold types showed minimal cell death compared to the control, and quantitative cell viability analysis revealed no significant differences among the groups (Fig. 3b). Cytoskeletal staining at the same time points demonstrated that chondrocytes on both scaffolds adopted a well-spread morphology (Fig. 3c); notably, by day 7, cells on PEXUU scaffolds were more uniformly distributed and denser, likely due to the scaffold's higher porosity and bioactivity. Cell proliferation, assessed via the CCK-8 assay (Fig. 3d), and quantitative DNA analysis (Fig. 3e) both confirmed that there were no significant differences among the groups. Overall, these results indicate that both PEUU and PEXUU scaffolds possess excellent biocompatibility with chondrocytes.

3.5. In Vitro anti-inflammatory performance evaluation of porous PEXUU scaffolds

PEXUU scaffolds were co-cultured with LPS-treated RAW264.7 macrophages to assess the expression of inflammation-related cytokines (TNF-α, IL-1β, and IL-6). Immunofluorescence staining (Fig. 4a) and quantitative fluorescence analysis (Fig. 4b–d) revealed that LPS stimulation significantly elevated cytokine expression compared to the control. Both the XN-only and PEXUU groups exhibited markedly reduced cytokine levels, suggesting that XN released from the PEXUU scaffold alleviates inflammation. In contrast, the PEUU group showed cytokine levels comparable to the LPS-only group.

RT-PCR analysis further confirmed that the mRNA expression of IL-6, IL-1β, and TNF-α was lower in the XN + LPS and PEXUU + LPS groups than in the LPS and PEUU + LPS groups (Fig. 4e and f). Additionally, analysis of the M1 marker INOS and the M2 marker CD206 (Fig. 4g–i) showed that LPS stimulation upregulated INOS and downregulated

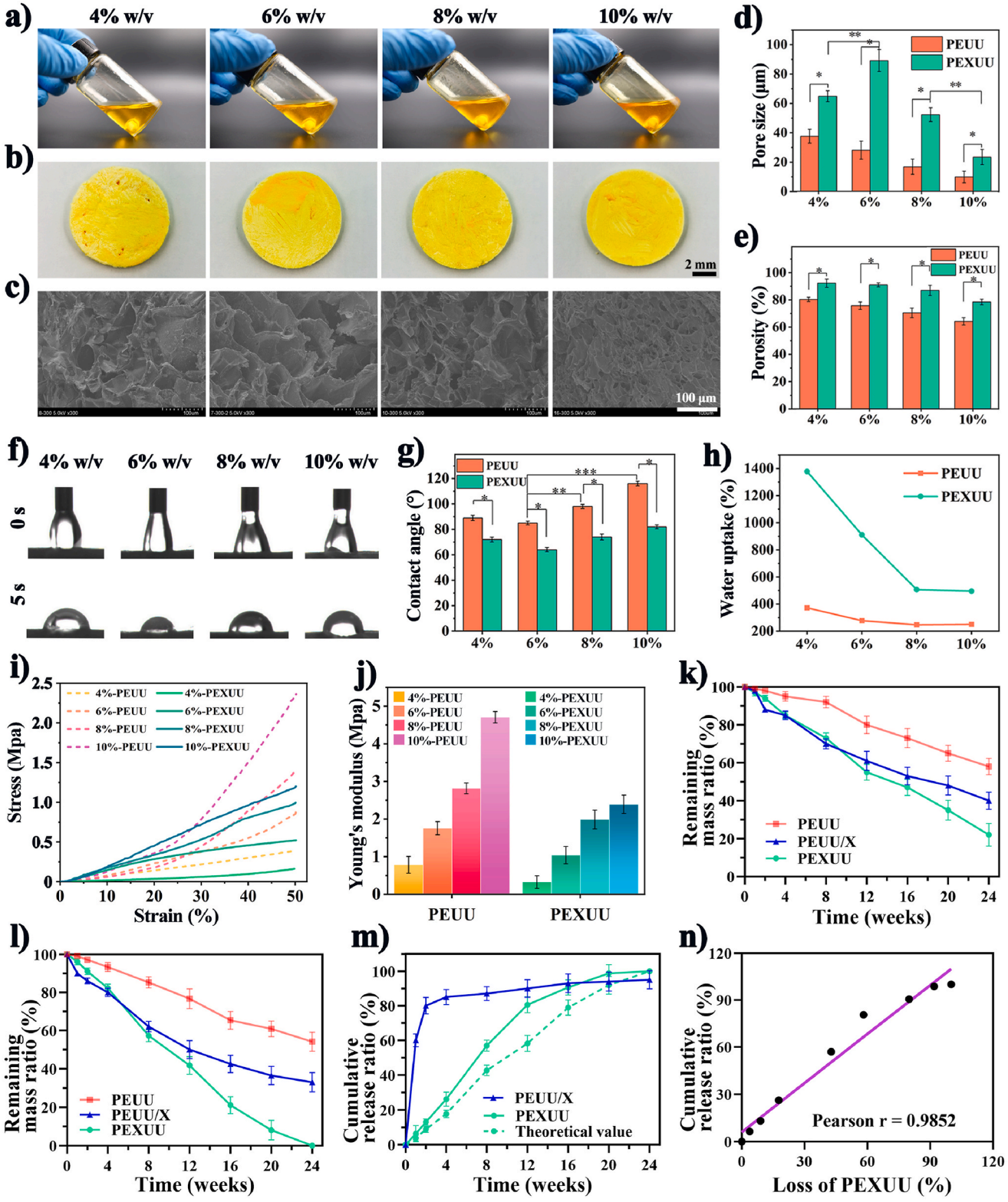

Fig. 2. Structure, Physicochemical Properties, and Degradation Behavior of PEXUU Porous Scaffolds. (a) PEXUU solutions prepared at varying concentrations. (b) Macroscopic morphology of PEXUU porous scaffolds at varying concentrations. (c) SEM images of PEXUU porous scaffolds at varying concentrations. (d) Pore size distribution of PEUU and PEXUU porous scaffolds at varying concentrations. (e) Porosity analysis of PEUU and PEXUU porous scaffolds at varying concentrations. (f) Water contact angle measurements of PEXUU scaffolds at 0 and 5 s. (g) Quantitative analysis of water contact angles for PEUU and PEXUU porous scaffolds at varying concentrations. (h) Water absorption tests for PEUU and PEXUU scaffolds at varying concentrations. (i) Stress–strain curves of PEUU and PEXUU scaffolds at varying concentrations. (j) Young's modulus of PEUU and PEXUU scaffolds at varying concentrations. (k) Hydrolytic degradation curves of PEUU, PEUU/X, and PEXUU scaffolds at a 6 % (w/v) concentration. (l) Enzymatic degradation curves of PEUU, PEUU/X, and PEXUU scaffolds at a 6 % (w/v) concentration. (m) Cumulative release curves of XN from PEUU/X and PEXUU scaffolds, including the theoretical cumulative release profile for XN from PEXUU scaffolds. (n) Correlation analysis between material degradation and XN release, indicating a significant positive correlation (r = 0.9852). Data represent mean ± SD (n = 5); *p < 0.05, **p < 0.01.

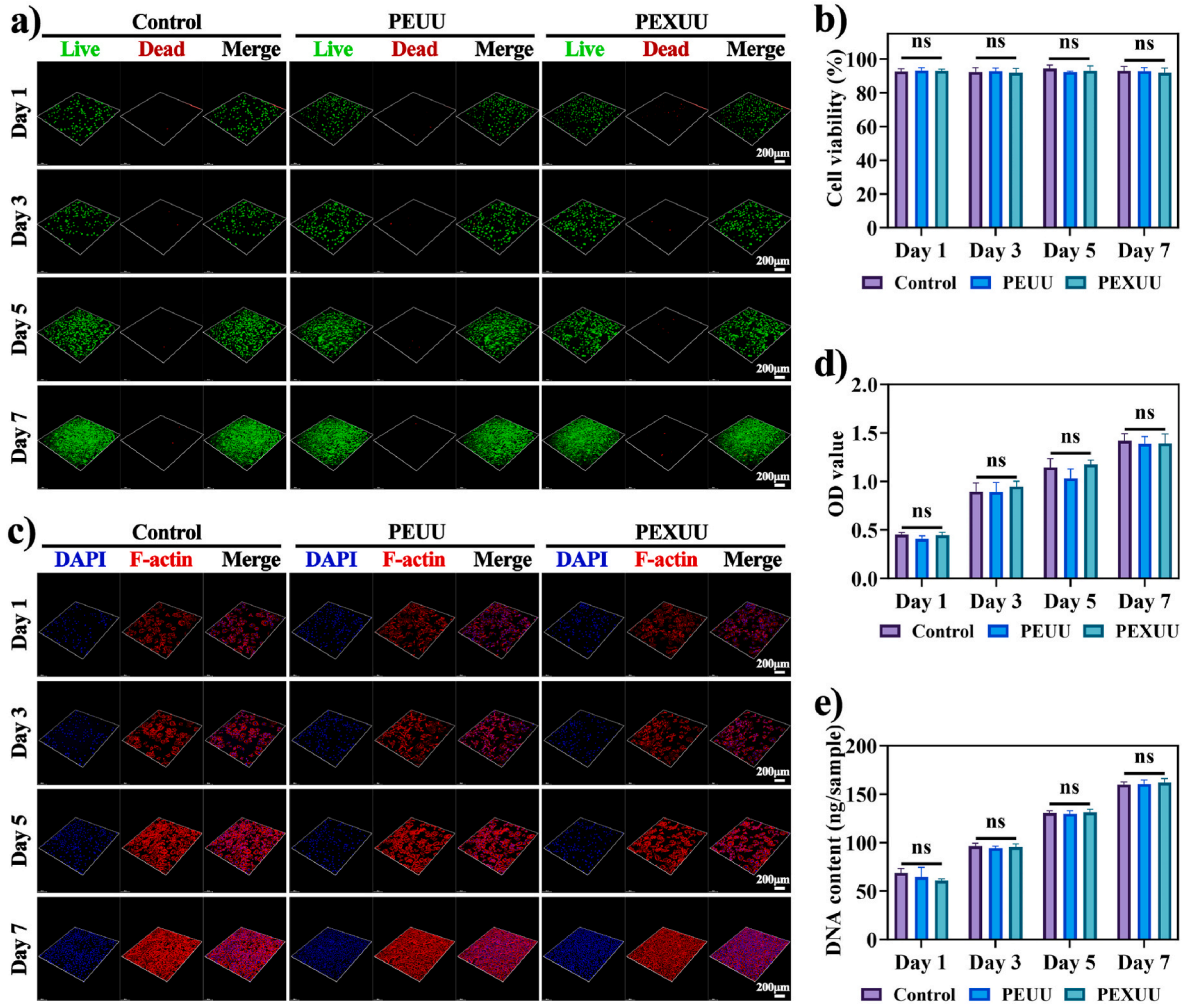

Fig. 3. *In Vitro* Biocompatibility Evaluation of Chondrocytes on PEUU and PEXUU Porous Scaffolds. (a) Live/dead staining of chondrocytes in the control, PEUU, and PEXUU groups after 1, 3, 5, and 7 days of culture. (b) Quantitative analysis of cell viability based on live/dead staining images for the control, PEUU, and PEXUU groups over 1, 3, 5, and 7 days. (c) Cytoskeletal staining of chondrocytes in the control, PEUU, and PEXUU groups after 1, 3, 5, and 7 days of culture. (d) OD measurements from the CCK-8 proliferation assay for the control, PEUU, and PEXUU groups at 1, 3, 5, and 7 days. (e) DNA content analysis of chondrocytes in the control, PEUU, and PEXUU groups after 1, 3, 5, and 7 days of culture. Data represent mean ± SD (n = 5); ns indicates no statistical significance.

CD206, thereby promoting a pro-inflammatory M1 phenotype. In contrast, both the XN + LPS and PEXUU + LPS groups significantly suppressed INOS expression while enhancing CD206 expression ($P < 0.01$), demonstrating favorable immunomodulatory capacity.

3.6. *In Vitro and In vivo cartilage formation*

Chondrocyte-seeded PEUU and PEXUU porous scaffolds were cultured *in vitro* for up to 4 weeks. After 2 weeks, gross observations (Fig. 5a) revealed that both groups maintained their initial morphology; however, histological staining showed only a few cartilage lacunae with limited ECM deposition, indicating an immature stage of cartilage formation. By 4 weeks (Fig. 5b), both groups exhibited a more mature, cartilage-like appearance with a smooth, translucent texture. Histological analysis revealed typical cartilage ECM deposition and numerous lacunae in both groups. Wet weight quantification (Fig. 5c) and quantitative analyses of GAG and COL II contents (Fig. 5c and d) showed no significant differences between the PEUU and PEXUU groups, suggesting that both scaffolds support *in vitro* cartilage formation comparably.

For the *in vivo* study, chondrocyte-seeded PEUU and PEXUU scaffolds were implanted subcutaneously in rabbits for 6 weeks. At 2 weeks, both groups exhibited a pale yellow appearance; however, histology revealed more extensive cartilage ECM deposition and lacunae formation in the PEXUU group (Fig. 5f). By 6 weeks (Fig. 5g), marked differences were evident: the PEUU group was covered with abundant vascularized connective tissue and lacked typical cartilage features, whereas the PEXUU group displayed the characteristic translucent white appearance of cartilage. Wet weight measurements (Fig. 5h) and quantitative analyses of GAG and COL II contents (Fig. 5i and j) confirmed that the PEXUU scaffold supported superior cartilage regeneration *in vivo* compared to the PEUU scaffold.

3.7. *In Vivo Anti-Inflammatory Performance evaluation*

Immunofluorescence staining was performed to assess the anti-inflammatory performance of the scaffolds. At week 2, the PEUU group exhibited significantly higher fluorescence intensities for CD68 and INOS—indicative of a predominance of M1 pro-inflammatory macrophages ($CD68^+/INOS^+$)—compared to the PEXUU group (Fig. 6a). In contrast, the PEXUU group showed lower CD68 and INOS expression. By week 6, the PEUU group's CD68 and INOS levels increased further, reflecting a persistent chronic inflammatory state (Fig. 6b), whereas the PEXUU group demonstrated a marked shift toward anti-inflammatory M2 macrophages ($CD68^+/CD206^+$). Quantitative analysis of fluorescence intensities supported these trends (Fig. 6c–e).

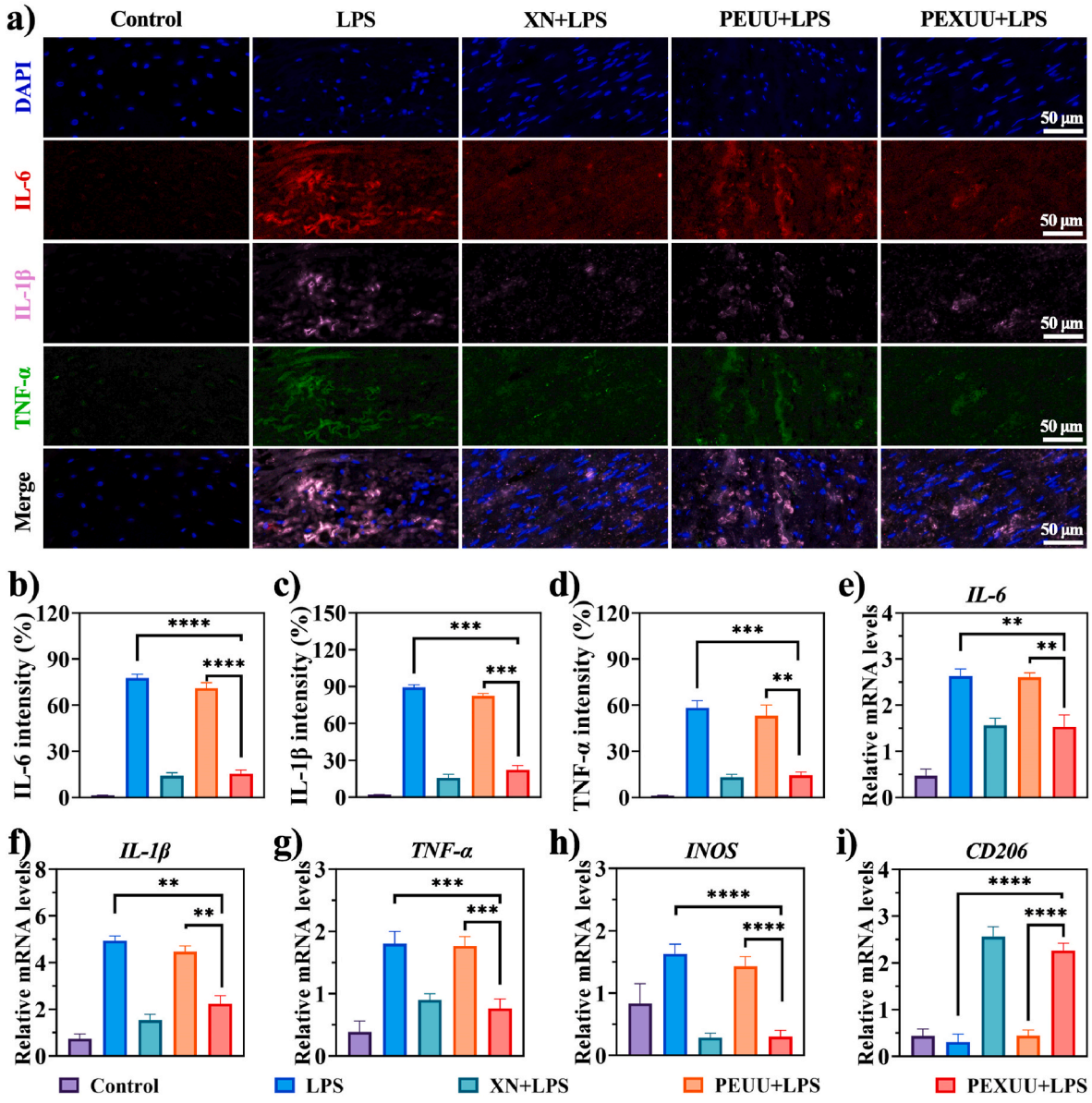

Fig. 4. *In Vitro* Evaluation of the Immunoregulatory Activities of PEXUU Scaffolds. (a) Immunofluorescence staining for IL-6, IL-1β, and TNF-α in RAW264.7 macrophages from five groups: control, LPS, XN + LPS, PEUU + LPS, and PEXUU + LPS. Quantitative analysis of immunofluorescence intensity for (b) IL-6, (c) IL-1β, and (d) TNF-α based on the staining images in the groups listed above. mRNA expression levels determined by RT-PCR for (e) *IL-6*, (f) *IL-1β*, (g) *TNF-α*, (h) *INOS*, and (i) *CD206* in the control, LPS, XN + LPS, PEUU + LPS, and PEXUU + LPS groups. Data represent mean ± SD (n = 5); **p < 0.01, ***p < 0.001, and ****p < 0.0001.

Furthermore, evaluation of inflammatory cytokines IL-1β and TNF-α at weeks 2 and 6 (Fig. 6f) revealed that at week 2, the PEUU group displayed strong fluorescence for both cytokines—especially TNF-α in areas of inflammatory cell aggregation—indicating a robust pro-inflammatory response. In contrast, the PEXUU group exhibited significantly lower fluorescence intensities. By week 6, IL-1β and TNF-α levels continued to rise in the PEUU group, while they decreased further in the PEXUU group—with almost no detectable TNF-α—indicating near-complete suppression of the inflammatory response. Quantitative fluorescence analysis confirmed these findings (Fig. 6g and h). These results demonstrate that the PEXUU scaffold effectively modulates immune responses and suppresses inflammation *in vivo*, thereby creating an anti-inflammatory microenvironment favorable for cartilage regeneration. Additionally, HE staining results revealed no detectable differences in the heart, liver, spleen, lung, and kidney tissues among the control, PEUU, and PEXUU groups (Fig. S6a–b), indicating that the synthesized PEXUU scaffold possesses satisfactory biosafety.

3.8. Tracheal repair using chondrocyte-loaded PEXUU scaffolds in a window-defect rabbit model

Tracheal repair was evaluated using a window-defect rabbit model, with bronchoscopy and tissue sampling conducted at 4 weeks. Gross observations revealed that the PEUU group failed to repair the tracheal defect—its repaired lumen was covered by granulation tissue and mucus—whereas the PEXUU group exhibited a relatively smooth and clear lumen (Fig. 7a). Bronchoscopic examination confirmed that the PEUU group's tracheal lumen was nearly collapsed with prominent granulation tissue, while the PEXUU group maintained an open lumen with a smooth surface and minimal granulation or mucus accumulation, aside from slight unevenness at the junction (Fig. 7b).

Postoperative survival analysis (Fig. 7c) showed that 70 % of rabbits in the PEXUU group survived, whereas all animals in the PEUU group died within 4 weeks due to respiratory distress from airway obstruction. Histological analysis of the repaired tracheal tissues using H&E and

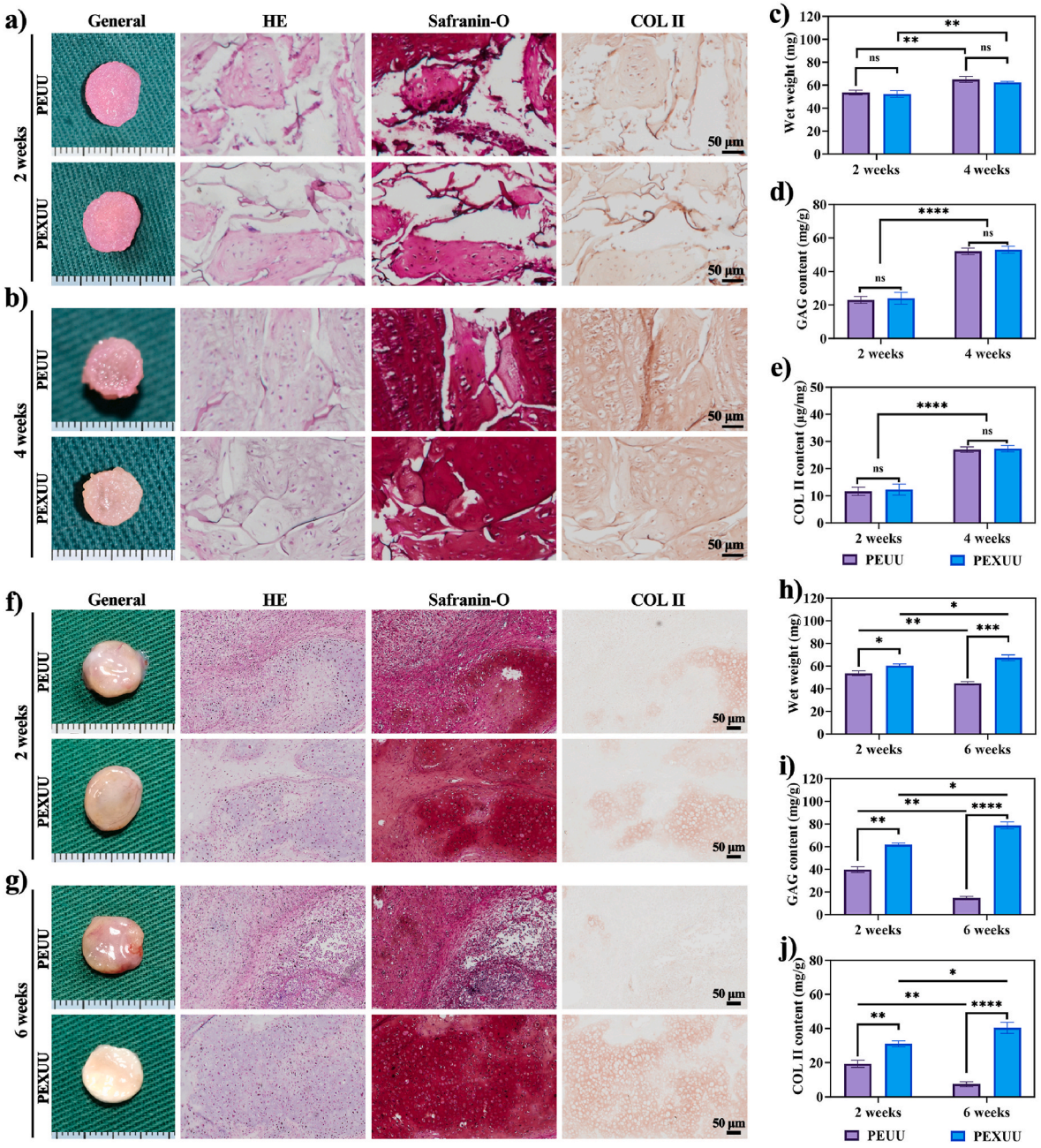

Fig. 5. *In Vitro* and *In Vivo* Evaluations of Cartilage Formation in PEUU and PEXUU Porous Scaffolds. (a–b) Representative macroscopic images, HE staining, Safranin-O staining, and COL II immunohistochemical staining of chondrocyte-loaded PEUU and PEXUU scaffolds after 2 and 4 weeks of *in vitro* culture. (c–e) Quantitative analyses of *in vitro* samples, including wet weight, GAG content, and COL II content, after 2 and 4 weeks of culture. (f–g) Representative macroscopic images, HE staining, Safranin-O staining, and COL II immunohistochemical staining of PEUU and PEXUU scaffolds following *in vivo* implantation for 2 and 6 weeks. (h–j) Quantitative analyses of *in vivo* samples, including wet weight, GAG content, and COL II content, after 2 and 6 weeks of implantation. Data represent mean ± SD ($n = 5$); *$p < 0.05$, **$p < 0.01$, ***$p < 0.001$, ****$p < 0.0001$; ns, no statistical significance.

Safranin O staining (Fig. 7d) revealed that the PEUU group contained abundant fibrous connective tissue with numerous inflammatory cells and negligible cartilage features, while the PEXUU group exhibited a smooth luminal surface with well-defined cartilage structures, including cartilage-specific ECM and typical lacunae. Quantitative analysis of COL II content (Fig. 7e) showed higher levels in the PEXUU group compared to the PEUU group, though still lower than in native tracheal tissue. Moreover, compression testing (Fig. 7f) indicated that the Young's modulus of the repaired tissue in the PEXUU group was comparable to normal cartilage and significantly higher than that in the PEUU group. Finally, immunofluorescence staining for COL II and cytokeratin (Fig. 7g) demonstrated that the PEUU group lacked both COL II deposition and epithelial tissue, whereas the PEXUU group showed abundant COL II and a measurable thickness of epithelial tissue. Collectively, these data indicate that the PEXUU porous scaffold substantially enhances tracheal defect repair compared to the PEUU scaffold.

4. Discussion

Current scaffolds for tracheal repair often fail to provide optimal outcomes due to insufficient mechanical adaptability and limited long-lasting anti-inflammatory properties. This study highlights the significant potential of PEXUU porous scaffolds in repairing tracheal defects,

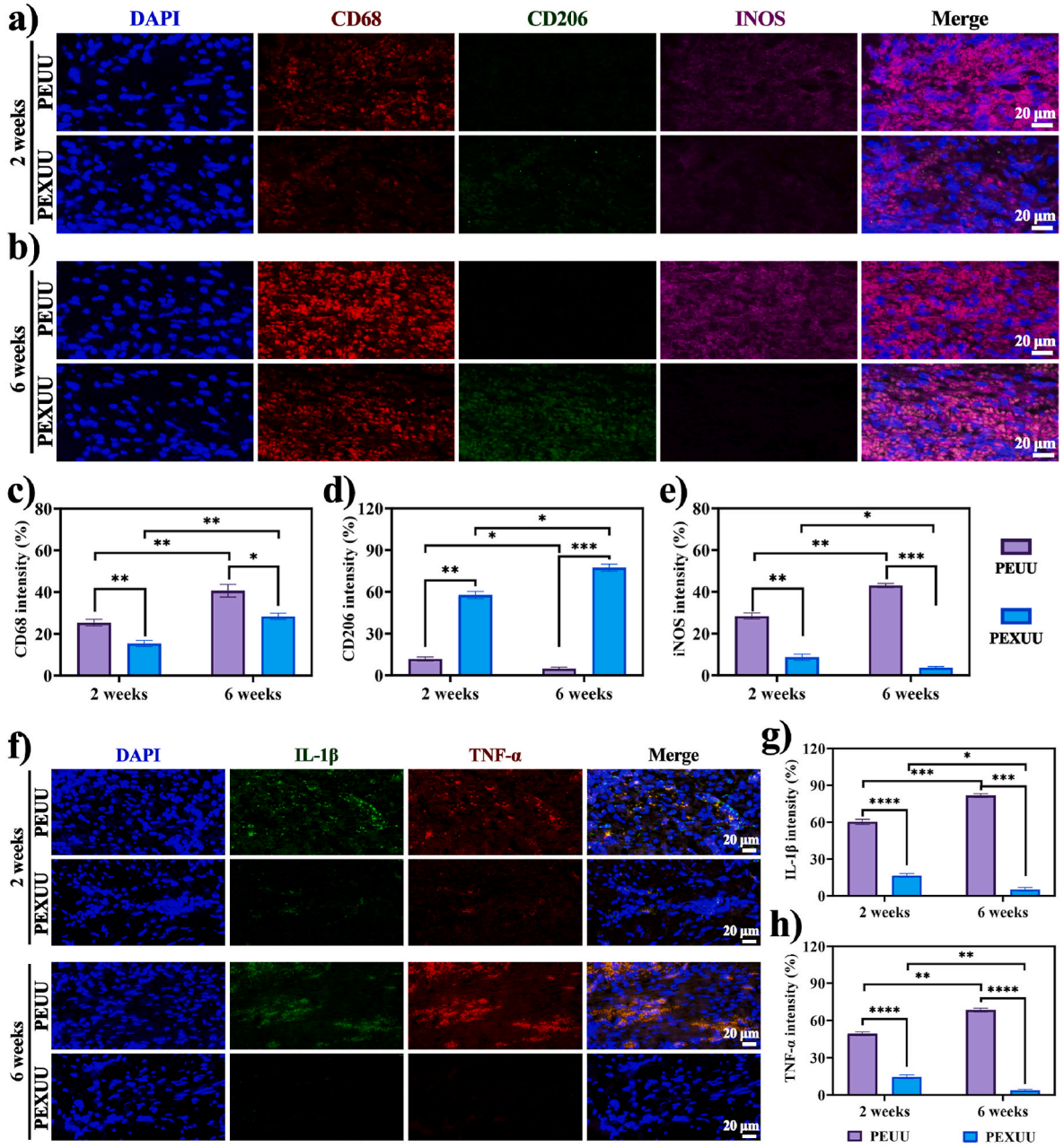

Fig. 6. *In Vivo* Anti-Inflammatory Performance of PEUU and PEXUU Porous Scaffolds. (a–b) Representative immunofluorescence staining images of macrophage markers CD68, CD206, and INOS in the PEUU and PEXUU groups after 2 and 6 weeks of implantation. (c–e) Quantitative analysis of the fluorescence intensities for CD68, CD206, and INOS in the PEUU and PEXUU groups at 2 and 6 weeks. (f) Representative immunofluorescence staining images of inflammatory cytokines IL-1β and TNF-α in the PEUU and PEXUU groups after 2 and 6 weeks of implantation. (g–h) Quantitative analysis of the fluorescence intensities for IL-1β and TNF-α in the PEUU and PEXUU groups at 2 and 6 weeks. Data represent mean ± SD (n = 5); *p < 0.05, **p < 0.01, ***p < 0.001, and ****p < 0.0001.

achieved through bulk-modification of XN into BDPU. The PEXUU scaffold offers favorable mechanical compliance featured with excellent elasticity and fatigue resistance that closely mimic natural trachea and effectively suppresses inflammation through the sustained drug release of XN, leading to enhanced repair of rabbit tracheal cartilage. This multifunctional scaffold provides an innovative solution for tracheal tissue engineering, combining mechanical adaptability with long-term anti-inflammatory bioactivity, thus holding great promise for future clinical applications.

Current tissue-engineered trachea scaffolds primarily utilize either natural or synthetic polymers, whereas both of them exhibit unmatched mechanical properties to normal trachea. The normal tracheal is mainly consisted of several C-type cartilage, and also includes interannular membranous and membranous ligaments rich in elastic fibers, which not only maintain the radial rigidity of the trachea (maintaining the patency of the duct) and longitudinal flexibility (conducive to flexible movements such as expansion, rotation and lateral bending), but also facilitate the diastolic and contractile activities caused by the cough reflex. Studies indicate that poor compliance of tracheal substitutes might be a primary cause leading to re-stenosis at the anastomotic site [30,31]. It is well known that rigidity is an essential property to maintain tracheal patency. The natural polymers are typical lack of sufficient rigidity to maintain the patency of tracheal lumen. In contrast, synthetic polymers can easily achieve the lateral stiffness well beyond the strength of the trachea. However, solely pursuing reliable rigid support creates a significant difference in stress between the tracheal substitutes and the

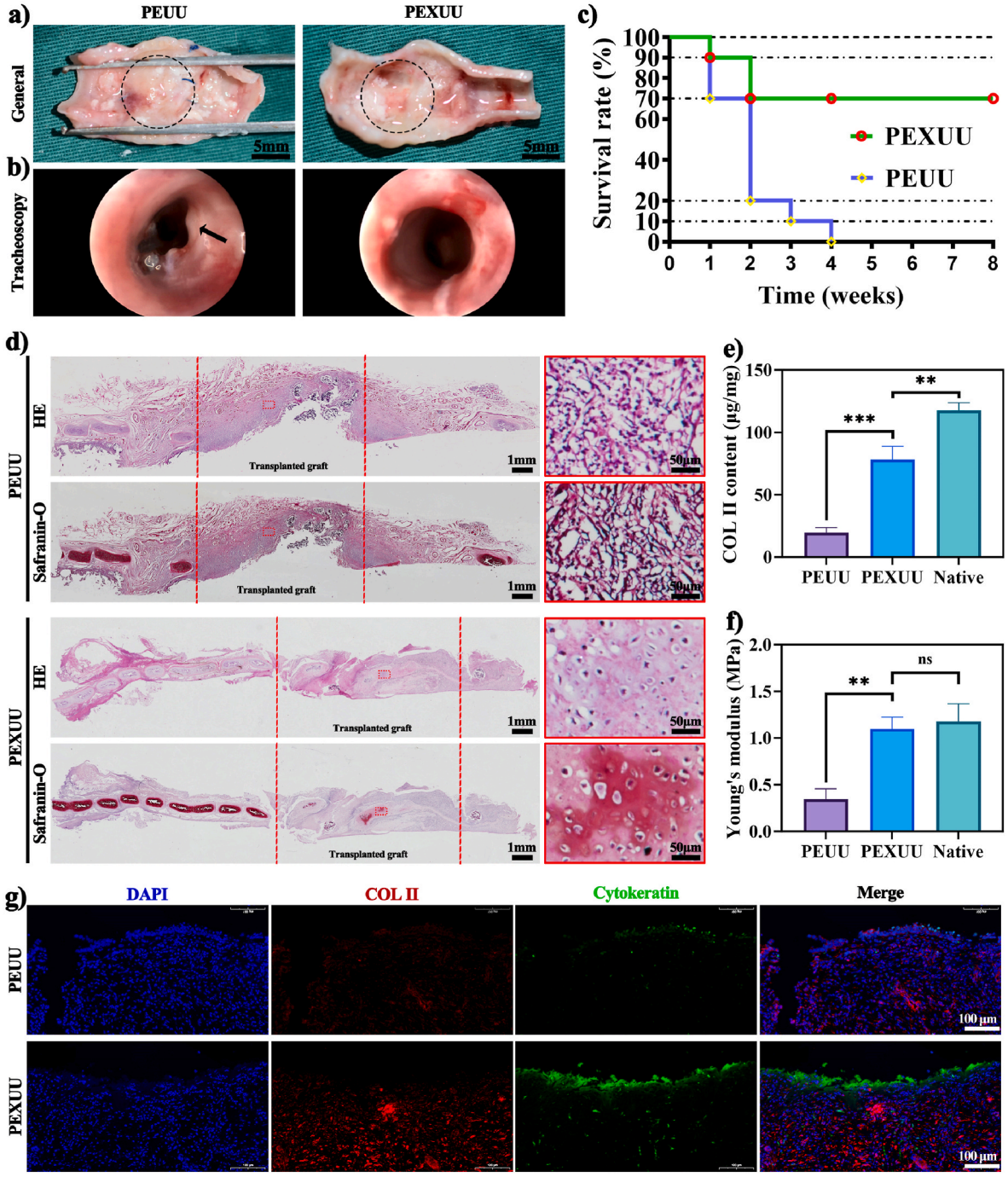

Fig. 7. Restoration Effects of PEUU and PEXUU Scaffolds in a Rabbit Tracheal Window-Defect Model. (a) Macroscopic images of the repaired trachea at 4 weeks in the PEUU and PEXUU groups. Black dotted circles highlight the window-defect area. (b) Tracheoscopy images of the repaired trachea at 4 weeks in the PEUU and PEXUU groups. Black arrows indicate regions with severe granulation tissue. (c) Post-operative survival rates of rabbits at 8 weeks in the PEUU and PEXUU groups. (d) Histological analysis of the repaired trachea at 4 weeks using HE and Safranin-O staining. Left panels show panoramic views of the entire repaired trachea, while right panels provide magnified images of the region outlined by rectangles. Dotted red lines delineate the repaired zones. (e) Quantitative analysis of COL II content in the repaired trachea for the PEUU, PEXUU, and native trachea groups at 4 weeks post-repair. (f) Quantitative measurement of Young's modulus in the repaired trachea for the PEUU, PEXUU, and native trachea groups at 4 weeks post-repair. (g) Immunofluorescence staining for COL II and Cytokeratin in the repaired trachea at 4 weeks in the PEUU and PEXUU groups. Data represent mean ± SD (n = 5); **p < 0.01, ***p < 0.001. (For interpretation of the references to color in this figure legend, the reader is referred to the Web version of this article.)

native trachea. Stiff scaffolds, in between breaths, cause friction with native trachea, fundamentally contributing to severe postoperative granulation tissue hyperplasia. Hence, enhancing the mechanical compliance of tracheal substitutes to eliminate stress on native trachea is crucial for preventing stenosis post-surgery [32].

Furthermore, the degradation of polyester materials like PLA and PGA releases acidic by-products, such as lactic acid and glycolic acid, which can directly damage cells and trigger innate immune responses. In addition, several other factors mentioned in our introduction section also pose significant inflammatory response to tracheal substitutes. These responses may activate macrophage polarization and the NLRP3 inflammasome pathway, leading to chronic inflammation and tissue

damage [33]. Hence, achieving a synergy between "mechanical compliance" and "anti-inflammatory" properties is crucial to overcoming the limitations of current biomaterials in tracheal repair.

BDPU, a biomaterial synthesized through the polymerization of polyol oligomers, diisocyanates, and chain extenders, demonstrates good biocompatibility and degradability. It can also be modified to meet specific requirements, making it widely used in medical applications. However, its use in trachea tissue engineering has been limited by its bioactivity, which is inferior to that of natural polymers. Improving its bioactivity for better applications in cartilage repair remains an ongoing research focus. Common drug delivery methods include physical coating and chemical grafting modifications [34]. Physical coating is simple but often results in short-duration release and drug burst. Chemical grafting, based on covalent bonding, offers more stable drug release but suffers from low drug loading efficiency due to the limited number of reactive groups on the material's surface. Over-activation of surface groups can also reduce the material's mechanical properties [35]. Given these limitations, there is an urgent need to explore a new drug delivery strategy for BDPU that can carry a high drug load while ensuring long-term, controlled release.

Bulk modification refers to the process of introducing small molecules with reactive groups during the initial synthesis of the material [36,37]. This approach replaces the original components, allowing the material to obtain biological activity without significantly altering its physicochemical properties. The resulting material can maintain biological activity over time before complete degradation. This promising modification strategy can harness the inherent biological characteristics of the raw material while avoiding damage caused by BDPU degradation. During degradation, the molecule bulk-modified BDPU can continuously release bioactive substances that regulate the microenvironment of the repair site.

XN, a flavonoid compound found in hops, has a prenyl group in its structure, providing strong anti-inflammatory properties. Previous studies have shown that XN reduces ECM degradation in chondrocytes and alleviates cartilage inflammation by inhibiting the activation of NF-κB in macrophages [38]. XN, with three active hydroxyl groups, can theoretically serve as a chain extender in BDPU synthesis, making it an effective candidate for functional bulk modification.

Molecular dynamics simulations and macro-mechanical testing suggest that partially replacing traditional chain extenders in the polyurethane elastomer with XN optimizes the flexibility of the main chain and intermolecular interactions. This enhances elasticity and fatigue resistance during cyclic compression and rebound tests. The introduction of the benzene ring structure significantly increases the stability of the molecular chains and improves the material's sustained support ability during simulated respiratory movements. This approach—focusing on both rigidity and flexibility—enables the scaffold to achieve a mechanical compliance comparable to that of natural trachea while maintaining excellent rebound and fatigue resistance, thus providing stable mechanical support for tracheal repair. Furthermore, the mechanical properties of the PEXUU scaffold are highly tunable. By adjusting the XN incorporation ratio and optimizing the soft-to-hard segment ratio, the rigidity, elasticity, and fatigue resistance of PEXUU can be customized. This design strategy ensures adequate mechanical support while aligning the scaffold's mechanical behavior with that of natural tracheal cartilage. Therefore, synthesizing functional PEXUU elastomers with adjustable mechanical properties using XN as a chain extender is theoretically feasible, which was also confirmed by this study.

XN is covalently embedded in the polyurethane main chain, enabling sustained drug release during material degradation. This process allows "degradation and drug release" to occur simultaneously. Traditional drug delivery systems often use surface coatings or physical adsorption to load drugs, which can face limitations in sustained release, drug loading efficiency, and *in vivo* stability [39,40]. In contrast, bulk modification with XN effectively avoids early drug burst release and insufficient drug loading later, ensuring continuous suppression of pro-inflammatory factors like TNF-α, IL-1β, and IL-6. Prolonged drug release reduces postoperative inflammation and fosters a reparative environment dominated by M2 macrophages, which promotes chondrocyte adhesion, proliferation, and differentiation. Moreover, the scaffold's degradation rate under enzymatic conditions correlates positively with the XN release curve, emphasizing that structural degradation drives uniform and sustained anti-inflammatory molecule release, which is crucial for addressing chronic inflammation and granulation tissue hyperplasia in long-segment tracheal defect repair.

When the synthesized PEXUU elastomers are returned to room temperature, they exhibit homogeneous gel-like consistency, with viscosity increasing in proportion to concentration. This suggests the PEXUU elastomers have a higher molecular weight and solubility limits, making them suitable for porous scaffold preparation via a TIPS method. The PEXUU scaffolds prepared using the TIPS method show higher porosity and uniform pore walls, ensuring interconnected pores in three-dimensional space. The 4 % and 6 % PEXUU scaffolds exhibit similar porosity (92.21 ± 2.98 % vs. 90.84 ± 2.45 %, no significant difference), but the 6 % group, with a wider pore size distribution and higher density, demonstrates superior material strength, beneficial for cartilage repair. These results indicate that the TIPS technique with a single solvent is ideal for processing PEXUU scaffolds with porous structures conducive to cell proliferation and nutrient exchange. Specifically, the 6 % group scaffold not only contains large pores that facilitate cell migration and nutrient exchange but also small pores that provide essential mechanical support, creating a hierarchical stress structure that reduces local stress concentrations and enhances mechanical performance [23].

Studies have shown that, compared to gas foaming or solvent casting methods, TIPS offers high adjustability, allowing precise control over pore structure while maintaining scaffold mechanical strength [41,42]. It also reduces potential chemical hazards to biocompatibility [43]. In terms of hydrophilicity, the contact angle of PEXUU scaffolds significantly decreases, promoting ECM protein adsorption and creating favorable conditions for chondrocyte extension and proliferation in the three-dimensional porous environment. Experimental observations reveal that the scaffold's pore morphology balances mechanical performance and cell permeability, facilitating nutrient and metabolic exchange essential for cartilage regeneration. The rational arrangement of the benzene ring structure and carbamate linkages, combined with the macroporous structure derived from TIPS, endows PEXUU with good hydrophilicity and high porosity, supporting mature cartilage tissue formation by chondrocytes both *in vitro* and *in vivo*.

The introduction of XN small molecules reduces the crosslinking degree of the hard segments in PEXUU, exposing more hydroxyl groups prone to hydrolytic degradation. This enhances the scaffold's hydrophilicity and water retention properties, increasing its contact area with water and accelerating material degradation. Enzymatic degradation significantly accelerates the breakdown of XN-modified polyurethane elastomers, suggesting that the enzymatic environment *in vivo* can enhance the degradation rate. This sustained release property aligns with the gradual increase in PEXUU's degradation rate, indicating that the degradation and drug release processes are closely intertwined. The XN-modified PEXUU scaffolds demonstrate ideal drug release capabilities. Notably, the actual XN release rate from PEXUU is slightly faster than theoretical predictions, particularly between weeks 12 and 24. Pearson correlation analysis shows a strong positive linear relationship between material mass loss during enzymatic degradation and cumulative XN release, further confirming that the XN release behavior is driven primarily by material degradation dynamics.

Both the XN-only group and the PEXUU group showed significantly reduced inflammatory cytokine expression, indicating that XN can reduce the inflammatory response of RAW264.7 macrophages. The anti-inflammatory effect in the PEXUU group was slightly weaker than in the XN-only group, but still significant, suggesting that XN-modified PEXUU

retains substantial anti-inflammatory activity. The PEUU group, lacking active drug components, shows a modest effect on LPS adsorption due to its microporous structure, leading to a slight reduction in inflammatory cytokine expression compared to the pure LPS group.

In *in vitro* and animal model tests, PEUU scaffold pose considerable inflammatory response. This activates the NF-κB/NLRP3 pathway [44], promoting the secretion of matrix metalloproteinases and accelerating the degradation of cartilage-specific ECM [45], ultimately leading to structural damage in engineered tracheal cartilage, manifested as fibrosis and granulation tissue hyperplasia [46]. In contrast, PEXUU promoted the distribution, growth, and ECM secretion of chondrocytes within the scaffold's three-dimensional structure, showing excellent cartilage regeneration in tracheal defect repair. Histological analysis and bronchoscopy revealed that the PEXUU group formed a substantial number of well-formed chondrocytes, maintaining tracheal lumen patency. These results suggest that incorporating anti-inflammatory active molecules into the molecular scaffold not only supports the mechanical demands of the natural trachea but also creates a favorable microenvironment for immune response regulation and ECM formation, providing solid support for chondrocyte growth and differentiation.

Despite significant advances in kinetic regulation, long-term anti-inflammatory effects, and cartilage repair, the study has some limitations. It primarily uses rabbit models, and the sample size and observation period may not fully represent the complex anatomical and immune characteristics of the human trachea. Safety evaluations of degradation by-products and their accumulation *in vivo* require further validation through long-term studies and larger animal models. Future research could explore the safety and long-term repair effects of PEXUU scaffolds in larger animal models, such as sheep or pigs, and investigate synergistic modification with other bioactive molecules, providing a more comprehensive foundation for clinical applications.

5. Conclusion

In summary, incorporating XN into BDPU yielded a porous scaffold (PEXUU) with tailorable mechanical properties and sustained anti-inflammatory activity. Simulation and mechanical testing confirmed that the XN modification enhanced chain flexibility and hydrogen bonding, resulting in elasticity and fatigue resistance comparable to natural trachea. The scaffold's high porosity, favorable hydrophilicity, and controlled XN release facilitated cartilage regeneration, promoted beneficial macrophage polarization, and effectively reduced inflammatory responses *in vitro*. Moreover, in a rabbit tracheal defect model, the PEXUU scaffold minimized granulation tissue formation, maintained luminal patency, and supported mature cartilage development. These results underscore the potential of XN-modified polyurethane with tailorable mechanical compliance and durable anti-Inflammatory efficacy for tracheal repair and highlight its promise for future clinical applications.

CRediT authorship contribution statement

Siqiang Zheng: Data curation, Conceptualization. **Li Xu:** Formal analysis, Investigation, Methodology. **Qitao Bo:** Funding acquisition, Formal analysis. **Erji Gao:** Supervision, Software. **Enkuo Zheng:** Methodology, Investigation. **Lei Xie:** Resources, Project administration. **Bin Zhao:** Software, Resources. **Jiaoyu Yi:** Visualization, Validation. **Yang Li:** Formal analysis, Data curation. **Yong Xu:** Writing – review & editing, Writing – original draft. **Yao Wang:** Investigation, Formal analysis. **Bo Tao:** Writing – review & editing, Funding acquisition.

Declaration of competing interest

The authors declare no conflict of interest.

Acknowledgments

The research was supported by the National Natural Science Foundation of China (82300068, and 82302395), and Shanghai Rising-Star Program (24QB2704800).

Appendix A. Supplementary data

Supplementary data to this article can be found online at https://doi.org/10.1016/j.mtbio.2025.101831.

Data availability

Data will be made available on request.

References

[1] W.H. Tseng, E.W. Liu, K.Y. Cheng, S.J. Wee, J.J. Lee, H.C. Chen, Tracheal replacement techniques and associated mortality: a systematic review, Laryngoscope 134 (4) (2024) 1517–1522.
[2] N. Xu, Y. Yuan, L. Ding, J. Li, J. Jia, Z. Li, D. He, Y. Yu, Multifunctional chitosan/gelatin@tannic acid cryogels decorated with in situ reduced silver nanoparticles for wound healing, Burns & Trauma 10 (2022).
[3] B.-S. Kim, J.-U. Kim, J. Lee, K.M. Ryu, S.-H. Kim, N.S. Hwang, Decellularized brain extracellular matrix based NGF-releasing cryogel for brain tissue engineering in traumatic brain injury, J. Contr. Release 368 (2024) 140–156.
[4] N. Panda, H.G. Auchincloss, Anatomy of the trachea, Thorac. Surg. Clin. 35 (1) (2025) 1–10.
[5] E.R. Gao, Y. Wang, P.L. Wang, Q.Y. Wang, Y.X. Wei, D.Y. Song, H.F. Xu, J.H. Ding, Y. Xu, H.T. Xia, R. Chen, L. Duan, C-shaped cartilage development using Wharton's jelly-derived hydrogels to assemble a highly biomimetic neotrachea for use in circumferential tracheal reconstruction, Adv. Funct. Mater. 33 (14) (2023).
[6] Y. Xu, J. Dai, X. Zhu, R. Cao, N. Song, M. Liu, X. Liu, J. Zhu, F. Pan, L. Qin, G. Jiang, H. Wang, Y. Yang, Biomimetic trachea engineering via a modular ring strategy based on bone-marrow stem cells and atelocollagen for use in extensive tracheal reconstruction, Adv. Mater. (Deerfield Beach, Fla.) 34 (6) (2022) e2106755.
[7] Y. Xu, Y.F. Guo, Y.Q. Li, Y.Y. Huo, Y.L. She, H. Li, Z.H. Jia, G.N. Jiang, G.D. Zhou, Z.W. You, L. Duan, Biomimetic trachea regeneration using a modular ring strategy based on poly(sebacoyl diglyceride)/polycaprolactone for segmental trachea defect repair, Adv. Funct. Mater. 30 (42) (2020).
[8] E. Gao, G. Li, R.F. Cao, H.T. Xia, Y. Xu, G.N. Jiang, K.Y. Xiao, J. Chen, R. Chen, L. Duan, Bionic tracheal tissue regeneration using a ring-shaped scaffold comprised of decellularized cartilaginous matrix and silk fibroin, Compos Part B-Eng 229 (2022).
[9] Y. Xu, H. Duan, Y.Q. Li, Y.L. She, J.J. Zhu, G.D. Zhou, G.N. Jiang, Y. Yang, Nanofibrillar decellularized Wharton's jelly matrix for segmental tracheal repair, Adv. Funct. Mater. 30 (14) (2020).
[10] R.A. Ilyas, M.Y.M. Zuhri, H.A. Aisyah, M.R.M. Asyraf, S.A. Hassan, E.S. Zainudin, S. M. Sapuan, S. Sharma, S.P. Bangar, R. Jumaidin, Y. Nawab, A.A.M. Faudzi, H. Abral, M. Asrofi, E. Syafri, N.H. Sari, Natural fiber-reinforced polylactic acid, polylactic acid blends and their composites for advanced applications, Polymers 14 (1) (2022) 202.
[11] N.G. Khouri, J.O. Bahú, C. Blanco-Llamero, P. Severino, V.O.C. Concha, E.B. Souto, Polylactic acid (PLA): properties, synthesis, and biomedical applications – a review of the literature, J. Mol. Struct. 1309 (2024) 138243.
[12] E. Mariani, G. Lisignoli, R.M. Borzì, L. Pulsatelli, Biomaterials: foreign bodies or tuners for the immune response? Int. J. Mol. Sci. 20 (3) (2019) 636.
[13] A. Osiecka-Iwan, A. Hyc, D.M. Radomska-Lesniewska, A. Rymarczyk, P. Skopinski, Antigenic and immunogenic properties of chondrocytes. Implications for chondrocyte therapeutic transplantation and pathogenesis of inflammatory and degenerative joint diseases, Cent. Eur. J. Immunol. 43 (2) (2018) 209–219.
[14] Y. Yao, C. Wang, Dedifferentiation: inspiration for devising engineering strategies for regenerative medicine, NPJ Regen. Med. 5 (1) (2020) 14.
[15] R. Li, J.J. Ye, L. Gan, M. Zhang, D. Sun, Y. Li, T. Wang, P. Chang, Traumatic inflammatory response: pathophysiological role and clinical value of cytokines, Eur. J. Trauma Emerg. Surg. 50 (4) (2024) 1313–1330.
[16] S. Liu, Z. Deng, K. Chen, S. Jian, F. Zhou, Y. Yang, Z. Fu, H. Xie, J. Xiong, W. Zhu, Cartilage tissue engineering: from proinflammatory and anti-inflammatory cytokines to osteoarthritis treatments (Review), Mol. Med. Rep. 25 (3) (2022) 99.
[17] Y. Liu, D. Li, Z. Yin, X. Luo, W. Liu, W. Zhang, Z. Zhang, Y. Cao, Y. Liu, G. Zhou, Prolonged in vitro precultivation alleviates post-implantation inflammation and promotes stable subcutaneous cartilage formation in a goat model, Biomed. Mater. 12 (1) (2017) 015006.
[18] E. Gao, P. Wang, F. Chen, Y. Xu, Q. Wang, H. Chen, G. Jiang, G. Zhou, D. Li, Y. Liu, L. Duan, Skin-derived epithelial lining facilitates orthotopic tracheal transplantation by protecting the tracheal cartilage and inhibiting granulation hyperplasia, Biomater. Adv. 139 (2022) 213037.
[19] Z. Cai, Y. Li, W. Song, Y. He, H. Li, X. Liu, Anti-inflammatory and prochondrogenic in situ-formed injectable hydrogel crosslinked by strontium-doped bioglass for cartilage regeneration, ACS Appl. Mater. Interfaces 13 (50) (2021) 59772–59786.

[20] R. Yu, Y. Yang, J. He, M. Li, B. Guo, Novel supramolecular self-healing silk fibroin-based hydrogel via host–guest interaction as wound dressing to enhance wound healing, Chem. Eng. J. 417 (2021) 128278.
[21] G. Zhou, H. Jiang, Z. Yin, Y. Liu, Q. Zhang, C. Zhang, B. Pan, J. Zhou, X. Zhou, H. Sun, D. Li, A. He, Z. Zhang, W. Zhang, W. Liu, Y. Cao, In vitro regeneration of patient-specific ear-shaped cartilage and its first clinical application for auricular reconstruction, EBioMedicine 28 (2018) 287–302.
[22] D.D. Pedersen, S. Kim, W.R. Wagner, Biodegradable polyurethane scaffolds in regenerative medicine: clinical translation review, J. Biomed. Mater. Res. 110 (8) (2022) 1460–1487.
[23] K. Dave, V.G. Gomes, Interactions at scaffold interfaces: effect of surface chemistry, structural attributes and bioaffinity, Mater. Sci. Eng. C 105 (2019) 110078.
[24] Y. Roth, D.Y. Lewitus, The grafting of multifunctional antithrombogenic chemical networks on polyurethane intravascular catheters, Polymers 12 (5) (2020) 1131.
[25] Y. Liu, L. Wang, Z. Liu, Y. Kang, T. Chen, C. Xu, T. Zhu, Durable immunomodulatory nanofiber niche for the functional remodeling of cardiovascular tissue, ACS Nano 18 (1) (2024) 951–971.
[26] J. Luo, Q. Pan, Y. Chen, W. Huang, Q. Chen, T. Zhao, Z. Guo, Y. Liu, B. Lu, Storage stability and degradation mechanism of xanthohumol in Humulus lupulus L. and beer, Food Chem. 437 (2024) 137778.
[27] C.M. Santos, A.M. Silva, The antioxidant activity of prenylflavonoids, Molecules 25 (3) (2020) 696.
[28] M. Stompor, B. Żarowska, Antimicrobial activity of xanthohumol and its selected structural analogues, Molecules 21 (5) (2016) 608.
[29] L.Q. Lin, Y.W. Xu, Y.Q. Li, X.D. Gong, M. Wei, W. Zhang, X. Zhang, Y. Xu, Nanofibrous Wharton's jelly scaffold in combination with adipose-derived stem cells for cartilage engineering, Mater. Des. 186 (2020).
[30] S. Kawaguchi, T. Nakamura, Y. Shimizu, T. Masuda, T. Takigawa, Y. Liu, H. Ueda, T. Sekine, K. Matsumoto, Mechanical properties of artificial tracheas composed of a mesh cylinder and a spiral stent, Biomaterials 22 (23) (2001) 3085–3090.
[31] J.F. Weber, S.S. Rehmani, M.Z. Baig, Y. Jadoon, F.Y. Bhora, Successes and failures in tracheal bioengineering: lessons learned, Ann. Thorac. Surg. 112 (4) (2021) 1089–1094.
[32] L. Guo, X. Liu, Y. Wang, J. Yi, J. Li, Y. Xu, K. Cai, W. Dai, Q. Feng, B. Tao, Enhancing long-segmental tracheal restoration: a self-repairing hydrogel loaded with chondrocytokines for sutureless anastomosis and cartilage regeneration, Mater. Today Bio 28 (2024) 101208.
[33] H. Chen, D.K. Agrawal, F.G. Thankam, Biomaterials-driven sterile inflammation, Tissue Eng Part B Rev 28 (1) (2022) 22–34.
[34] W. Zhang, Y. Zhang, Z. Hao, P. Yao, J. Bai, H. Chen, X. Wu, Y. Zhong, D. Xue, Synthetic nanoparticles functionalized with cell membrane-mimicking, bone-targeting, and ROS-controlled release agents for osteoporosis treatment, J. Contr. Release 378 (2025) 306–319.
[35] H. Xiao, M. Aliabouzar, M.L. Fabiilli, Acoustically responsive scaffolds: unraveling release kinetics and mechanisms for sustained, steady drug delivery, J. Contr. Release 374 (2024) 205–218.
[36] Y. Li, B. Qiu, Z. Li, X. Wang, Z. He, D.M. Sandoval, R. Song, A. Sigen, C. Zhao, M. Johnson, J. Lyu, I. Lara-Sáez, W. Wang, Backbone cationized highly branched poly(β-amino ester)s as enhanced delivery vectors in non-viral gene therapy, J. Contr. Release 367 (2024) 327–338.
[37] G. Kiran Raj, E. Singh, U. Hani, K.V.R.N.S. Ramesh, S. Talath, A. Garg, K. Savadatti, T. Bhatt, K. Madhuchandra, R.A.M. Osmani, Conductive polymers and composites-based systems: an incipient stride in drug delivery and therapeutics realm, J. Contr. Release 355 (2023) 709–729.
[38] E. Oledzka, Xanthohumol-A miracle molecule with biological activities: a review of biodegradable polymeric carriers and naturally derived compounds for its delivery, Int. J. Mol. Sci. 25 (6) (2024).
[39] T. Chen, Y. Jiang, J.-P. Huang, J. Wang, Z.-K. Wang, P.-H. Ding, Essential elements for spatiotemporal delivery of growth factors within bio-scaffolds: a comprehensive strategy for enhanced tissue regeneration, J. Contr. Release 368 (2024) 97–114.
[40] J. Chen, J. Luo, J. Feng, Y. Wang, H. Lv, Y. Zhou, Spatiotemporal controlled released hydrogels for multi-system regulated bone regeneration, J. Contr. Release 372 (2024) 846–861.
[41] R. Zeinali, L.J. Del Valle, J. Torras, J. Puiggali, Recent progress on biodegradable tissue engineering scaffolds prepared by thermally-induced phase separation (Tips), Int. J. Mol. Sci. 22 (7) (2021) 3504.
[42] F.C. Pavia, F.S. Palumbo, V. La Carrubba, F. Bongiovì, V. Brucato, G. Pitarresi, G. Giammona, Modulation of physical and biological properties of a composite PLLA and polyaspartamide derivative obtained via thermally induced phase separation (TIPS) technique, Mater. Sci. Eng. C 67 (2016) 561–569.
[43] R. Akbarzadeh, A.M. Yousefi, Effects of processing parameters in thermally induced phase separation technique on porous architecture of scaffolds for bone tissue engineering, J. Biomed. Mater. Res Part B: Appl. Biomater. 102 (6) (2014) 1304–1315.
[44] Y. Mu, L. Wang, L. Fu, Q. Li, Knockdown of LMX1B suppressed cell apoptosis and inflammatory response in IL-1β-induced human osteoarthritis chondrocytes through NF-κB and NLRP3 signal pathway, Mediators Inflamm 2022 (2022) 1870579.
[45] Y. Sha, B. Zhang, L. Chen, C. Wang, T. Sun, Dehydrocorydaline accelerates cell proliferation and extracellular matrix synthesis of TNFα-treated human chondrocytes by targeting Cox2 through JAK1-STAT3 signaling pathway, Int. J. Mol. Sci. 23 (13) (2022) 7268.
[46] W. Zhao, F. Xu, Y. Shen, Q. Ding, Y. Wang, L. Liang, W. Dai, Y. Chen, Temporal control in shell-core structured nanofilm for tracheal cartilage regeneration: synergistic optimization of anti-inflammation and chondrogenesis, Regen. Biomater. 11 (2024) rbae040.